LABORATORY STUDIES ON THE IRRADIATION OF METHANE IN INTERSTELLAR, COMETARY, AND SOLAR SYSTEM ICES

CHRIS J. BENNETT,[1] COREY S. JAMIESON,[1] YOSHIHIRO OSAMURA,[2] AND RALF I. KAISER[1,3]

ABSTRACT

Pure methane ices (CH_4) were irradiated at 10 K with energetic electrons to mimic the energy transfer processes that occur in the track of the trajectories of MeV cosmic-ray particles. The experiments were monitored via an FTIR spectrometer (solid state) and a quadrupole mass spectrometer (gas phase). Combined with electronic structure calculations, this paper focuses on the identification of CH_x ($x = 1-4$) and C_2H_x ($x = 2-6$) species and also investigates their formation pathways quantitatively. The primary reaction step is determined to be the cleavage of a carbon-hydrogen bond of the methane molecule to form a methyl radical (CH_3) plus a hydrogen atom. Hydrogen atoms recombined to form molecular hydrogen, the sole species detected in the gas phase during the irradiation exposure. In the matrix two neighboring methyl radicals can recombine to form an internally excited ethane molecule (C_2H_6), which either can be stabilized by the surrounding matrix or was found to decompose unimolecularly to the ethyl radical (C_2H_5) plus atomic hydrogen and then to the ethylene molecule (C_2H_4) plus molecular hydrogen. The initially synthesized ethane, ethyl, and ethylene molecules can be radiolyzed subsequently by the impinging electrons to yield the vinyl radical (C_2H_3) and acetylene (C_2H_2) as degradation products. Upon warming the ice sample after the irradiation, the new species are released into the gas phase, simulating the sublimation processes interstellar ices undergo during the hot core phase or comets approaching perihelion. Our investigations also aid the understanding of the synthesis of hydrocarbons likely to be formed in the aerosol particles and organic haze layers of hydrocarbon-rich atmospheres of planets and their moons such as Titan.

Subject headings: astrochemistry — cosmic rays — ISM: molecules — methods: laboratory — molecular processes — planets and satellites: general

Online material: color figures

1. INTRODUCTION

Interstellar methane (CH_4) is thought to be formed on the surface of interstellar ices, where hydrogen atoms can combine with a carbon atom sequentially (d'Hendecourt et al. 1985). Indeed, methane is known to be ubiquitous throughout the interstellar medium, where it has been detected in both the gas phase and solid state (Lacy et al. 1991). A recent survey of 23 infrared sources, mostly young stellar objects and field stars, carried out by Gibb et al. (2004) using the *Infrared Space Observatory* (*ISO*) detected methane in interstellar ices via its ν_4 deformation mode at 7.676 μm (1303 cm^{-1}). The abundance of methane within these ices was found to be typically 1%–4% relative to water; however, upper limits of 13% and 17% were reported for Mon R2 IRS 3 and GCS 4, respectively. The band position and profile was found to be consistent with the methane molecule being within a polar matrix such as water. It is also well established that the icy grains present within interstellar clouds are subjected to irradiation from Galactic cosmic rays originating from supernovae explosions; these particles have high kinetic energies up to the GeV; for instance, 1 MeV particles have fluxes of $\phi = 10$ particles cm^{-2} s^{-1} (Strazzulla & Johnson 1991). Chemically speaking, the cosmic-ray radiation field comprises about 98% protons (p, H^+) and 2% helium nuclei (α-particles, He^{2+}). The cosmic-ray particles also induce an internal ultraviolet radiation field ($\lambda < 13.6$ eV), hold-

ing a fluence of $\phi = 10^3$ photons cm^{-2} s^{-1} (Prasad & Tarafdar 1983). The effects of this high-energy radiation exposure over the lifetime of an interstellar cloud of about $(4-6) \times 10^8$ yr (Jones 2005) is expected to produce significant chemical alterations of the ices condensed on the grain nuclei (Kaiser 2002). The production of new hydrocarbons formed from the irradiation of methane in the solid state and their subsequent ejection into the gas phase as the ice sublimes also has profound consequences for chemical models of interstellar cores (Ruffle & Herbst 2001).

Studying the chemical composition of comets may also provide a record of the "pristine material" of the parent interstellar cloud from which our solar system was formed (Ehrenfreund et al. 2004). Hydrocarbons including methane (CH_4), ethane (C_2H_6), and acetylene (C_2H_2) have been detected as they sublimed from the interior of the long period comets including C/1996 B2 Hyakutake, C/1995 O1 Hale-Bopp with abundances relative to water ranging from 0.5%–1.5%, 0.6%, and 0.2%–0.3% (Brooke et al. 1996; Mumma et al. 1996, 2003; Weaver et al. 1999, respectively). It has been suggested that the formation of ethane and acetylene are likely to have originated from the irradiation of methane within interstellar ices; indeed, the idea has already been studied within a water-dominated matrix (Moore & Hudson 1998).

Methane is also found to be abundant throughout the solar system (Ehrenfreund & Charnley 2000; Roush 2001). Other than the Earth, which obviously has biogenic sources today, it has been detected within the atmospheres of Mars (<0.02 ppm), Jupiter (1000 ppm), Saturn (2000 ppm), Uranus (0.003–0.01 ppm), and Nepune (0.015 ppm). Trace amounts of ethane, ethylene, and acetylene have been detected within the atmospheres of these planets as well (Cruikshank 1998). Observations of Titan with *ISO* by Coustenis et al. (2003) also revealed the presence of a few

[1] Department of Chemistry, University of Hawai'i at Manoa, Honolulu, HI 96822; kaiser@gold.chem.hawaii.edu
[2] Department of Chemistry, Rikkyo University, 3-34-1 Nishi-ikebukuro, Tokyo 171-8501, Japan.
[3] Department of Physics and Astronomy, Open University, Walton Hall, Milton Keynes MK7 6AA, UK.

percent of methane, as well as minor traces of associated hydrocarbons including ethane (C_2H_6), ethylene (C_2H_4), acetylene (C_2H_2), propane (C_3H_8), allene (H_2CCCH_2), methylacetylene (CH_3CCH), diacetylene ($HCCCCH$), and benzene (C_6H_6). Infrared studies of outer solar system icy bodies like Pluto with the United Kingdom Infrared Telescope (UKIRT) verified from the position of the methane band that methane molecules are not only embedded in solid nitrogen (N_2) dominated ices but also as islands of solid methane (Douté et al. 1999).

Previous experiments studying the effects of both ultraviolet (UV) photolysis and irradiation by ions on solid methane have been carried out; however, little information regarding a quantitative interpretation of the results exists. Gerakines et al. (1996) exposed pure ice samples of about 0.1 μm thickness (including methane) to UV irradiation from a microwave discharge flow lamp; typically, the flux of photons is estimated to be 10^{15} photons cm^{-2} s^{-1} with energies greater than 6 eV, but predominantly, the photons produced are Lyα photons (10.2 eV). The products were studied via mid-infrared spectroscopy, whereby they identified the methyl radical (CH_3), ethane, propane, and ethylene, as well as characteristic absorptions indicating the presence of larger hydrocarbons containing double and triple bonds. The detection of acetylene was not reported. Later, Kaiser & Roessler (1998) exposed methane ice targets of about 4 μm thickness to irradiation from both 9.0 MeV α-particles and 7.3 MeV protons. Again, by the use of infrared spectroscopy, the authors found that the chemical alterations were slightly different from those by UV irradiation; notably, they reported the formation of acetylene as well as several previously undetected radical species, methylene (CH_2), the ethyl radical (C_2H_5), and the vinyl radical (C_2H_3). More recently, Baratta et al. (2002) prepared thin samples around 7.40 nm thick, and compared the effects of photons generated via a hydrogen discharge resonance lamp (Lyα photons) and 30 keV ions at currents ranging from 100 nA cm^{-2} to a few μA cm^{-2}. The chemical alteration of the ices was monitored by infrared spectroscopy, but the study was focused on the destruction of methane and production of only ethane and propane, whereby few other species were mentioned. They found that at low doses, the irradiation effects from both sources were comparable, but at higher doses the optical properties of the ice hindered the further processing by UV photons. Moore & Hudson (2003) also recently studied the effects of both UV photons generated from a microwave-discharged hydrogen flow lamp as well as 0.8 MeV protons generated by a Van de Graff generator on pure methane ice (several microns thick). The products were studied using infrared spectroscopy, whereby only a qualitative approach was taken to analyze the effects of radiolysis on the methane sample, whereby the acetylene molecule was found to be produced in both experiments (note that in a previous study by Gerakines et al. [1996], the same peaks were listed as present but unidentified), yet in contrast to previous studies, ethylene and propane were not identified in the UV photolyzed samples. Thus, it is clear that further work is needed to establish how differing radiation sources chemically alter these ices. To our knowledge, however, no previous experiments studying the irradiation effects of high-energy electrons on solid methane under ultrahigh vacuum conditions have been carried out. The choice of energetic electrons as an irradiation source serves to simulate not only the irradiation of icy surfaces by energetic electrons (e.g., the Jovian system) but also the effects of δ electrons released in the track of an MeV ion trajectory (see Bennett et al. [2005] for more details). The linear energy transfer through electronic interactions to the ice sample from keV electrons is also of the same order to that of MeV ions. The focus of this paper is the production mechanisms of small hydrocarbons (where C_xH_y [$x \leq 2, y \leq 6$]).

2. EXPERIMENTAL

Briefly, an ultrahigh vacuum (UHV) chamber is evacuated down to a base pressure of typically 5×10^{-11} torr using oil-free magnetically suspended turbomolecular pumps. A closed cycle helium refrigerator is used to cool a highly polished silver (111) mono crystal to 11.0 ± 0.3 K, which is held in the center of the chamber and is freely rotatable. The methane (CH_4) frost was prepared by depositing methane (99.999%, Specialty Gas Group) through a glass capillary array held 5 mm from the silver target for 5 minutes at a background pressure in the main chamber of 10^{-7} torr. A Nicolet 510 DX Fourier transform infrared spectrometer (242 scans over 5 minutes from $6000-400$ cm^{-1}, resolution 2 cm^{-1}) running in absorption-reflection-absorption mode (reflection angle $\alpha = 75°$) is used to monitor the condensed sample. A quadrupole mass spectrometer (Balzer QMG 420) operating in residual gas analyzer mode with the electron impact ionization energy at 90 eV allows us to detect any species in the gas phase during the experiment.

The methane samples were irradiated isothermally at 11.0 ± 0.3 K with 5 keV electrons generated with an electron gun (Specs EQ 22–35) at beam currents of 100 nA for 1 hr by scanning the electron beam over an area of 1.8 ± 0.3 cm^2. In theory this would mean during the irradiation the sample would be exposed to a total of 2.2×10^{15} electrons (1.2×10^{15} electrons cm^{-2}); however, not all of the electrons generated by our electron gun actually reach the target; the manufacturer states an extraction efficiency of 78.8%, meaning the actual number of electrons which hit the sample is reduced to 1.8×10^{15} electrons (9.8×10^{14} electrons cm^{-2}). After the irradiation is complete, the sample is then left isothermally for an hour before heated to 300 K at a rate of 0.5 K minute^{-1}.

Figure 1 depicts a typical infrared spectrum of the condensed methane frost prior to the irradiation at 11 K; the assignments of these bands are presented in Table 1. At this temperature, methane is orientated in its phase II crystalline structure, which is stable below 20.4 K. Indeed, the fine structure arising from the ν_3 and ν_4 fundamental bands is consistent with that of phase II methane (which have some hindered motion), with some amorphous features portrayed by additional fine structure not attributable to that of phase II methane. There have been numerous studies on the structure of methane in phase II, and the corresponding infrared assignments (Chapados & Cabana 1972; Kobashi et al. 1977; Baciocco et al. 1987a, 1987b; Khanna & Ngoh 1990; Grieger et al. 1998).

The column density of methane (molecules cm^{-2}) can be calculated via a modified Lambert-Beers relationship as in equation (1) (see Bennett et al. [2004] for more details);

$$N = \frac{\ln 10}{2} \cos \alpha \frac{\int_{\tilde{\nu}_1}^{\tilde{\nu}_2} A(\tilde{\nu}) \, d\tilde{\nu}}{A}, \qquad (1)$$

where the division by a factor of 2 corrects for the ingoing and outgoing infrared beam, α is the angle between the normal of the surface mirror, and the infrared beam, $\int_{\tilde{\nu}_1}^{\tilde{\nu}_2} A(\tilde{\nu}) \, d\tilde{\nu}$ is the integral of the infrared absorption feature for our sample (per centimeter), and A is the integral absorption coefficient (in centimeter per molecule), often referred to as an "A-value." Because of the large number of expected products and complicated fine structure of the strongly absorbing fundamental ν_3 and ν_4 bands, it is logical to use the overtone/combination bands to determine the column density of the methane sample. Using a recently determined
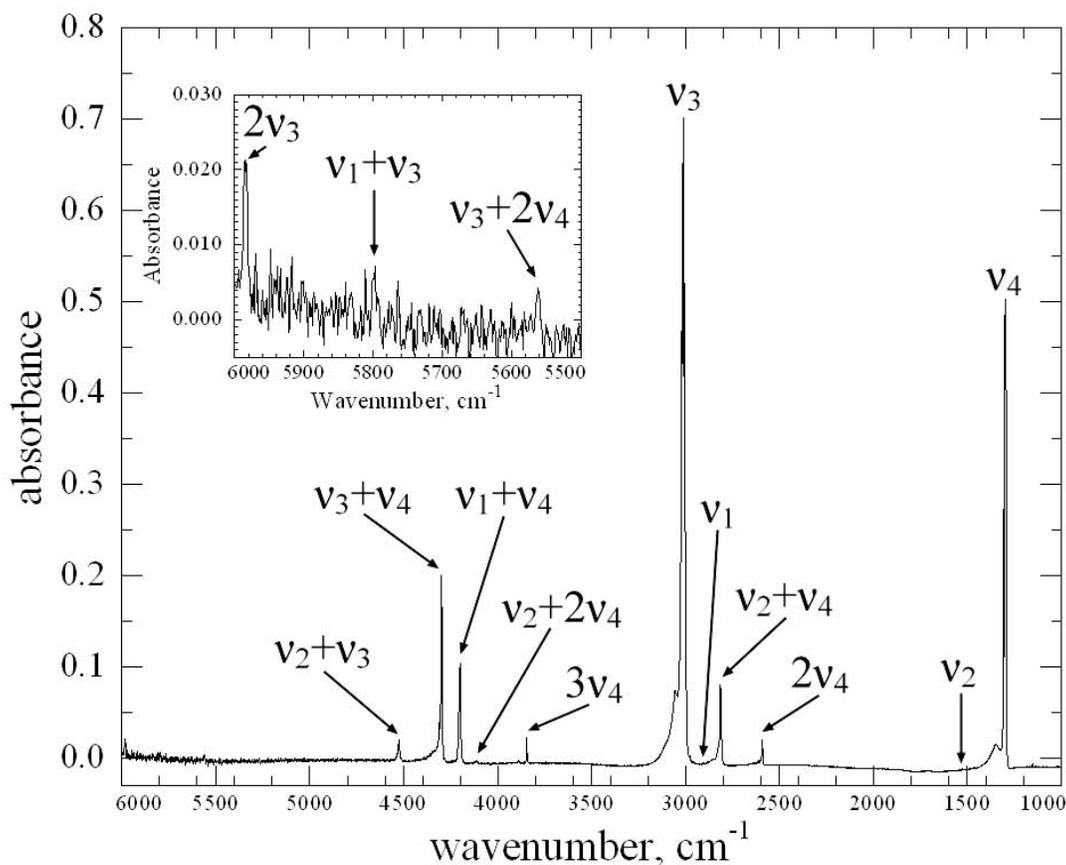
Fig. 1.—Infrared spectrum of the methane frost at 11 K. The range 6000–5500 cm^{-1} has been enlarged to show the less intense combination bands. The corresponding assignments are given in Table 1.

A-value from Gerakines et al. (2005) of 1.6×10^{-18} cm molecule^{-1} for the combination band appearing at 4200 cm^{-1} ($\nu_1 + \nu_4$), we derive a column density of $2.29 \pm 0.05 \times 10^{17}$ molecules cm^{-2}. Taking a density of 0.53 g cm^{-3} (Wyckoff 1965), we can derive a thickness of 115 ± 2 nm. The electron trajectories were simulated using the CASINO code (Drouin et al. 2001). The results indicate that the distribution maximum for the energy of electrons after they have been transmitted through the sample is 4.63 ± 0.01 keV,

which means that they transfer a total of 370 ± 10 eV into the sample. This value corresponds to an average linear energy transfer (LET) of 3.2 ± 0.1 keV μm^{-1}, and therefore exposing our sample to an *average* dose of 1.6 ± 0.2 eV per molecule.

3. RESULTS

Figure 2 shows the optimized molecular structures of the species relevant to this study (see Appendix for details). Figure 3

TABLE 1

INFRARED ABSORPTIONS OF THE METHANE FROST AND ASSIGNMENTS OF THE OBSERVED BANDS

Band Position (cm^{-1})	Assignment	Characterization
5984	$2\nu_3$	Overtone
5799	$\nu_1 + \nu_3$	Combination
5562	$\nu_3 + 2\nu_4$	Combination
4525, 4527	$\nu_2 + \nu_3$	Combination
4284, 4298, 4309, 4311, 4322, 4336, 4384	$\nu_3 + \nu_4$	Combination
4119, 4202	$\nu_1 + \nu_4$	Combination
4115	$\nu_2 + 2\nu_4$	Combination
3843, 3845	$3\nu_4$	Overtone
3001, 3005, 3013, 3015, 3019, 3025, 3052, 3065	ν_3	Fundamental
2904, 2918	ν_1	Fundamental
2800, 2812, 2814, 2822, 2827, 2849, 2884	$\nu_2 + \nu_4$	Combination
2576, 2591, 2597, 2612, 2630	$2\nu_4$	Overtone
1523, 1528	ν_2	Fundamental
1289, 1294, 1299, 1304, 1307, 1345	ν_4	Fundamental

NOTE.—Absorptions and assignments are done according to Chapados & Cabana (1972) and Baciocco et al. (1987a, 1987b).
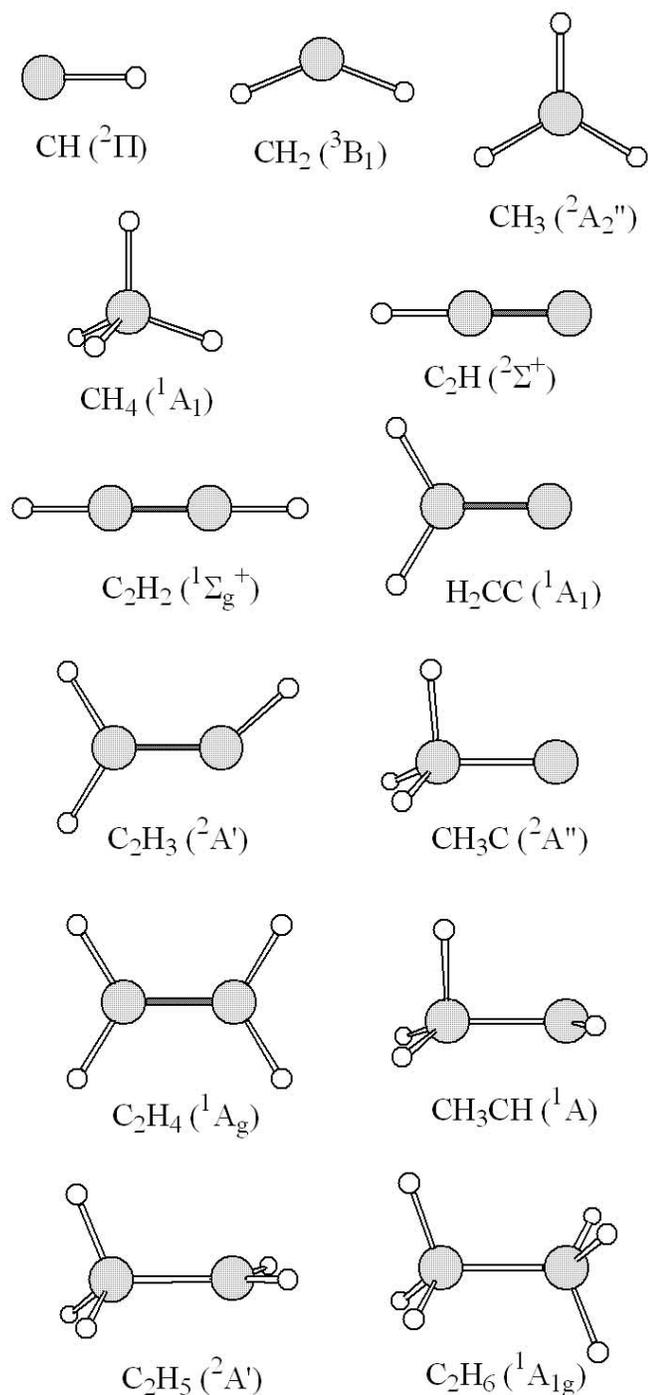
Fig. 2.—Structures of various hydrocarbons determined with the B3LYP/6-311G(d,p) method (see text for details).

shows the infrared spectrum after irradiation exposure compared to the neat ice sample. A list of the species identified along with the corresponding assignments is shown in Table 2. The temporal evolution of the column densities of these species are shown in Figures 4a–4g with the corresponding quantitative information listed in Table 3. Note that during the 1 hr irradiation period, the infrared bands were fit using Gaussian curves, which allows for greater accuracy in determining the peak areas than the direct band integration used in the subsequent isothermal and heating stages, which accounts for the apparent onset of jagged features in Figures 4a–4g after the irradiation period has elapsed. Taking meth-

ane as an example, the temporal development of the column density was observed by its $\nu_1 + \nu_4$ combination band at 4200 cm^{-1} and is shown in Figure 4a using the A-value of 1.6×10^{-18} cm molecule^{-1} (Gerakines et al. 2005). After irradiation the column density is calculated to be $2.18 \pm 0.04 \times 10^{17}$ molecules cm^{-2}; recall that the initial column density was found to be $2.29 \pm 0.05 \times 10^{17}$ molecules cm^{-2}; this means that the amount of methane molecules destroyed during irradiation is found to be $1.15 \pm 0.63 \times 10^{16}$ molecules cm^{-2}, i.e., only about 5%. Taking into account that 9.8×10^{14} electrons cm^{-2} hit the target, we can calculate that each electron destroys 11.7 ± 6.4 methane molecules on average. The column density of methane remains constant over the isothermal period where the sample is kept at 11 K for 1 hr, and then once the temperature program is started, begins to decrease as the sample is heated, in which the entire methane matrix sublimated rapidly from 39–42 K.

Note also that this paper is focusing on the formation of only C$_2$H$_x$ ($x = 1$–6) and CH$_y$ ($y = 1$–4) species. As most of these features have been previously identified in irradiation experiments on methane ice, we shall only discuss those that are reported for the first time. In regards to ethane (X $^1A_{1g}$), the bands at 2941 and 2915 cm^{-1} are tentatively assigned to the infrared active combination bands arising from the combination of the $\nu_8 + \nu_{11}$ modes ($E_u \otimes E_g = A_{1u} \oplus A_{2u} \oplus E_u$) allowing two infrared active bands (Nakamoto 1997; Hepp & Herman 1999); the relative intensities of these bands of about 4 : 1 is the same as in pure ethane samples from our laboratory data (Fig. 3c). These bands have been assigned to ethane previously by Gerakines et al. (1996) at 2942 and 2908 cm^{-1}, respectively. It is also expected that there will be a slight contribution to the band appearing at 2961 cm^{-1} from the infrared inactive band ν_1 (CH$_3$ symmetric stretch); however, the major contributor to this bands is likely to be from higher hydrocarbons such as propane (C$_3$H$_8$). Note that Gerakines et al. (1996) assigned a band appearing at 2908 cm^{-1} to ethane, which is not present in the pure sample. A more likely explanation is that during irradiation, the amount of amorphous methane increases; this reduces the site symmetry of the methane molecules to C$_1$, making all vibrations infrared active; hence, here we assign this band to the ν_1 band of methane (Fig. 3c).

The isomer of ethylene, CH$_3$-CH(X $^3A''$), could not be identified unambiguously; the most intense bands from our density functional theory (DFT) calculations are from the fundamentals ν_9 at 2889 cm^{-1} and ν_3 at 2855 cm^{-1}, both of around the same intensity. There are two bands occurring at 2851 and 2834 cm^{-1}, which are consistent with these observations (a shift of 20–40 cm^{-1} for absorptions in the solid state is not uncommon), but due to the low intensities of these bands, the assignment can only be tentative.

Note that several species remain unidentified. These include the methylene radical, CH$_2$(X $^3B_1$), whereby the strongest absorption, the ν_2 bending mode, is not particularly strong ($A \sim 2 \times 10^{-18}$ cm molecule^{-1}) and is predicted by our calculations to absorb at 1024 cm^{-1}. However, experimental results using tunable diode laser spectroscopy and laser magnetic resonance techniques place the absorption closer to 963 cm^{-1} (Marshall & McKellar 1986), a feature that would be hard to observe next to the intense absorptions from ethylene and higher hydrocarbons that also absorb in this region. The feature previously reported by Kaiser & Roessler (1998) at 1109 cm^{-1} to be the methylene radical was also not found to be present in our electron-irradiated sample. Similarly, the vinylidene isomer, H$_2$CC(X $^1A_1$), which is unlikely to be identified as the strongest band (ν_4 at 728 cm^{-1}), overlaps with the strong ν_5 band from acetylene and could not be observed. Although
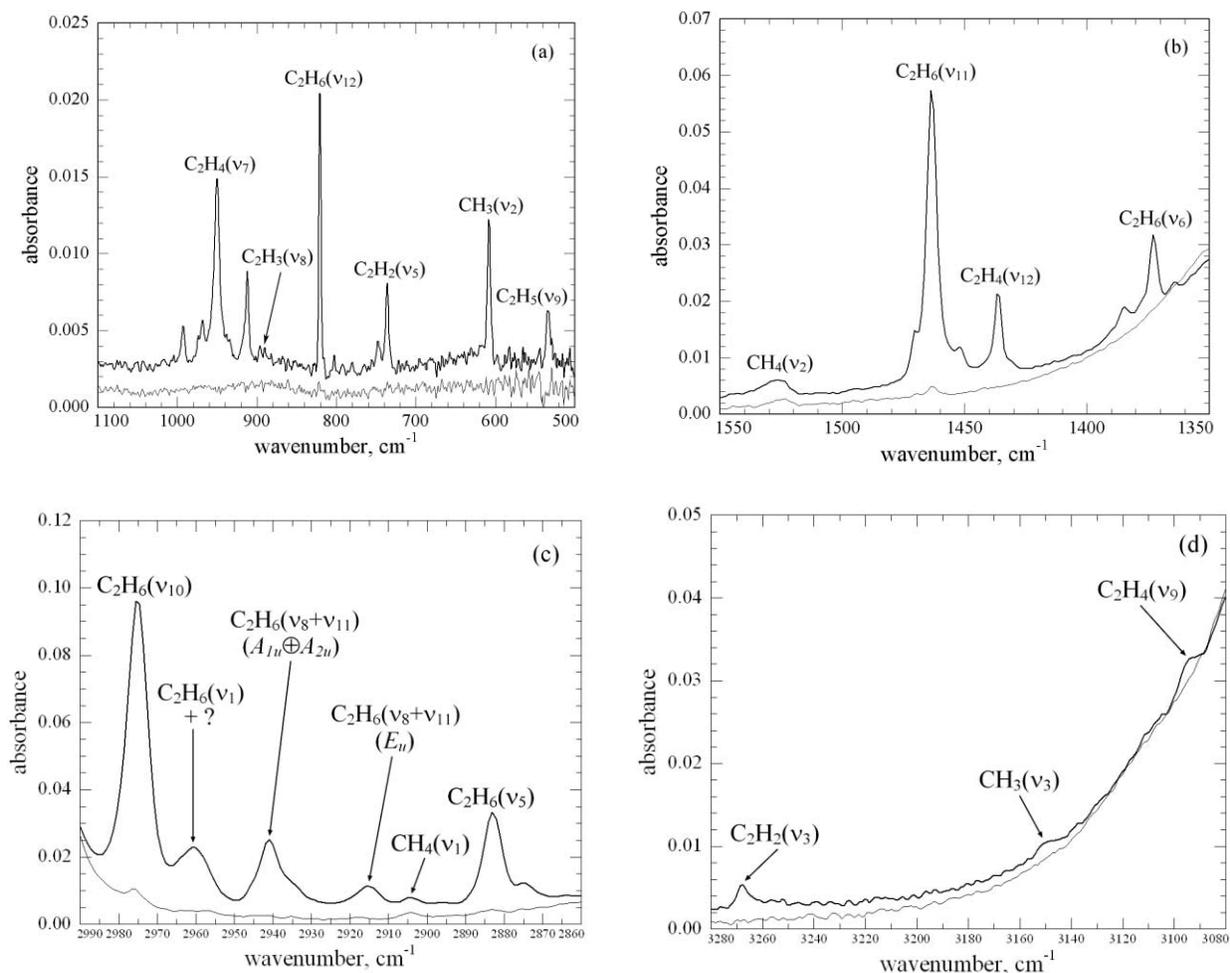
Fig. 3.—Infrared spectrum of the methane sample before irradiation (*gray lines*), and after 60 minutes of irradiation with 5 keV electrons at 0.1 μA (*black lines*), within the ranges (a) $1100-500$ cm^{-1}, (b) $1550-1350$ cm^{-1}, (c) $2990-2860$ cm^{-1}, and (d) $3280-3080$ cm^{-1}. The assignments are compiled in Table 2.

TABLE 2

Observed Peak Positions, Assignments, and Characterizations after 1 hr of Irradiation

Band Position (cm^{-1})	Literature Values			Assignment	Characterization
	Gerakines et al. (1996)	Moore & Hudson (2003)	Kaiser & Roessler (1998)		
608....................	608	608	609	ν_2 CH$_3$	Out of plane
3150[a]....................				ν_3 CH$_3$	CH stretching
2961[b]....................				ν_1 C$_2$H$_6$	CH$_3$ sym. str.
2883....................	2882	2883		ν_5 C$_2$H$_6$	CH$_3$ sym. str.
1373....................	1375	1373		ν_6 C$_2$H$_6$	CH$_3$ sym. def.
2975....................	2975	2976		ν_{10} C$_2$H$_6$	CH$_3$ deg. str.
1464....................	1465	1463		ν_{11} C$_2$H$_6$	CH$_3$ d-deform
822....................	822	821		ν_{12} C$_2$H$_6$	CH$_3$ rock
2941[c]....................				$\nu_8 + \nu_{11}$ C$_2$H$_6$	Combination
2915[c]....................				$\nu_8 + \nu_{11}$ C$_2$H$_6$	Combination
534....................		534	534	ν_9 C$_2$H$_5$	CH$_2$ out of plane
951....................			951	ν_7 C$_2$H$_4$	CH$_2$ wag
1435....................		1438	1436	ν_{12} C$_2$H$_4$	CH$_2$ scissor
3095....................		3095		ν_9 C$_2$H$_4$	CH$_2$ asym. str.
2851[d]....................				ν_9 CH$_3$CH	CH$_2$ asym. str.
2834[d]....................				ν_3 CH$_3$CH	CH$_3$ sym. str.
893....................			898	ν_8 C$_2$H$_3$	Out of plane
3267....................		3269	3261	ν_3 C$_2$H$_2$	CH stretch
736....................			735	ν_5 C$_2$H$_2$	CH bend

Notes.—Observations are via 5 keV electrons at 0.1 μA, together with the calculated values for the integrated absorption coefficients used in this paper. Tentative assignments are given in italics.
[a] Also reported by Snelson (1970) and Pacansky & Bargon (1975) at 3162 and 3150 cm^{-1}, respectively.
[b] Not the major contributing species to the band (see text for details).
[c] Assignment supported by work from Nakamoto (1997) as well as Hepp & Herman (1999).
[d] Assignment based on calculated band positions of these species (see Appendix).
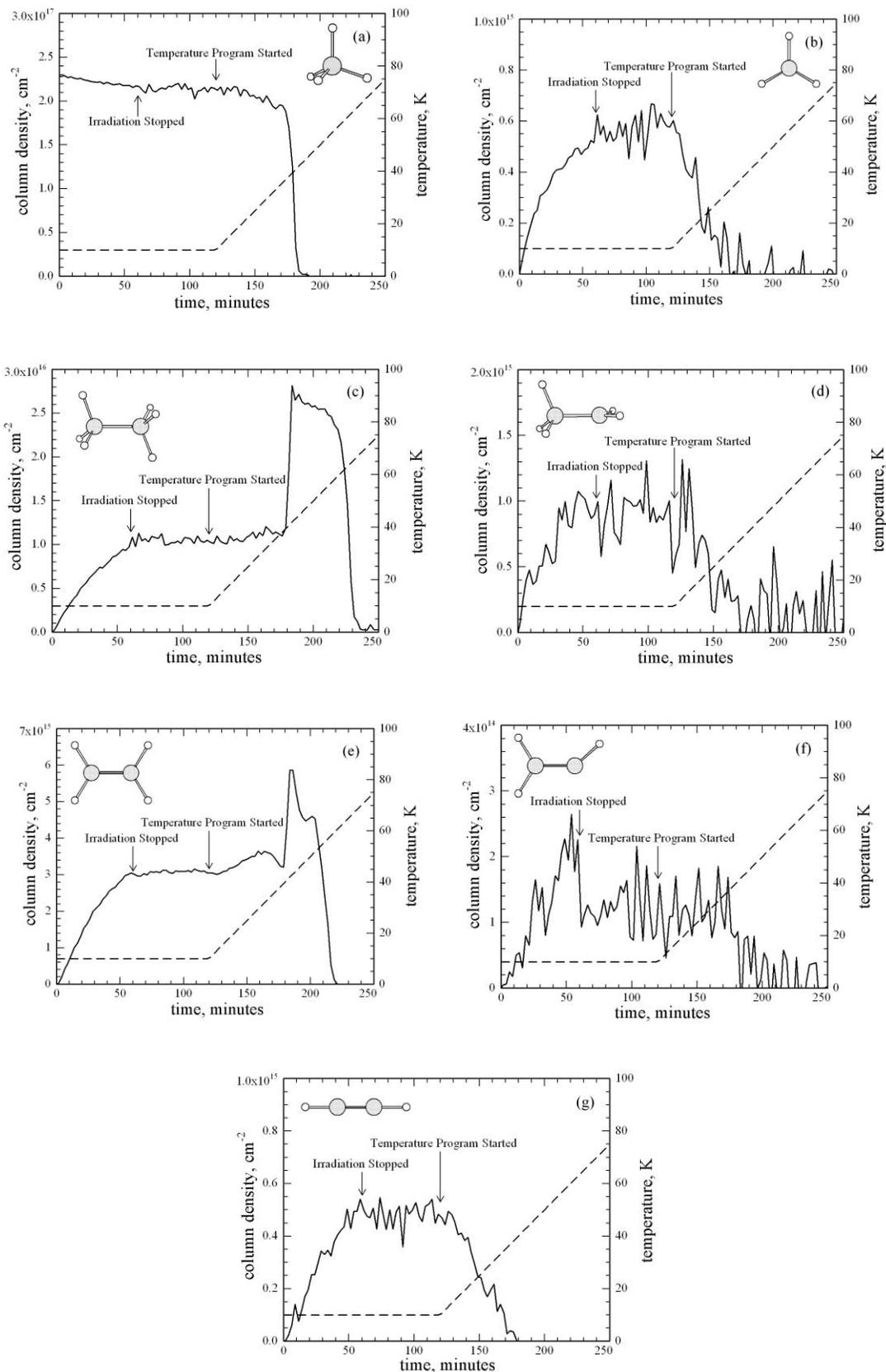
Fig. 4.—Temporal development of the column densities calculated from the corresponding integrated absorptions (*a*) methane at 4200 cm^{-1}, (*b*) the methyl radical at 608 cm^{-1}, (*c*) ethane at 822 cm^{-1}, (*d*) the ethyl radical at 535 cm^{-1}, (*e*) ethylene at 950 cm^{-1}, (*f*) the vinyl radical at 895 cm^{-1}, and (*g*) acetylene at 736 cm^{-1}. Error bars have been omitted for clarity. The corresponding temperature profile is overlaid (*dashed line*).

TABLE 3

SUMMARY OF TEMPORAL CHANGES IN COLUMN DENSITY OF THE OBSERVED SPECIES

Species	Wavenumber (cm^{-1})	A (cm molecule^{-1})	Change in Column Density over Irradiation (molecules cm^{-2})	Number of Molecules Produced per Electron[a]	Sublimation Temperature (K)
CH$_4$.....................	4200	1.6×10^{-18}[b]	$(-1.15 \pm 0.63) \times 10^{16}$	-11.7 ± 6.4	$39-42$
CH$_3$.....................	608	2.5×10^{-17}[c]	$(5.16 \pm 0.30) \times 10^{14}$	0.52 ± 0.03	<35
C$_2$H$_6$	822	1.9×10^{-18}[d]	$(9.66 \pm 0.24) \times 10^{15}$[e]	9.82 ± 0.24	$57-66$
C$_2$H$_5$	534	9.3×10^{-18}[f]	$(9.0 \pm 1.5) \times 10^{14}$	0.91 ± 0.15	<25
C$_2$H$_4$	951	1.5×10^{-17}[g]	$(3.05 \pm 0.10) \times 10^{15}$	3.10 ± 0.10	$52-60$
C$_2$H$_3$	893	1.3×10^{-17}[f]	$(2.3 \pm 0.8) \times 10^{14}$	0.23 ± 0.08	<40
C$_2$H$_2$	736	1.4×10^{-17}[h]	$(5.24 \pm 0.41) \times 10^{14}$	0.53 ± 0.04	$15-40$

NOTES.—Summary is based on the indicated band position and the corresponding A-value at the end of irradiation and the number of molecules produced per incident electron. The temperature at which the species sublimated from the matrix is also indicated.
[a] Based on 9.8×10^{14} electrons cm^{-2} hitting the target (see § 2).
[b] Value from Gerakines et al. (2005).
[c] Value from Wormhoudt & McCurdy (1989).
[d] Value from Pearl et al. (1991).
[e] Note that a minor quantity of ethane is present as impurity in our pure gas.
[f] Calculated value (see Appendix).
[g] Value from Cowieson et al. (1981).
[h] Value from Kaiser & Roessler (1998).

searched for, the vinylidyne isomer CH$_3$C(X $^2A''$) nor the ethynyl radical C$_2$H($X^2\Sigma^+$) could not be identified in these experiments.

4. DISCUSSION

4.1. Reaction Scheme

We now attempt to kinetically fit the column densities of the new species produced on irradiation of the sample. During this discussion, we refer to the reactions listed in Table 4 (R1)–(R18), which underlie the chemical processes considered for the reaction scheme; the summary of this scheme is shown in Figure 5. Considering the experimentally observed column density of methane, we assumed that the molecule undergoes first-order "decay" on electron bombardment, similar to a radioactive decay, giving the following rate (eq. [2]). This equation can be used to fit the column density of the methane molecule during the irradiation phase via equation (3). The best fit of the methane profile yields [CH$_4$]$(t = 0) = 2.29 \pm 0.01 \times 10^{17}$ molecules cm^{-2} and $k_a = 1.62 \pm 0.07 \times 10^{-5}$ s^{-1} and is shown in Figure 6. To fit the experimentally observed column density of the methyl radical, assuming it is produced via reaction (R1), a first order growth (eq. [4]) can be expected. The best-fit results from this equation yields $a = 5.43 \pm 0.08 \times 10^{14}$ molecules cm^{-2} and $k_b = 7.84 \pm 0.31 \times 10^{-4}$ s^{-1} (Fig. 6).

$$-d[\text{CH}_4]/dt = k_a[\text{CH}_4], \qquad (2)$$

$$[\text{CH}_4](t) = [\text{CH}_4](t = 0)e^{-k_a t}, \qquad (3)$$

$$[\text{CH}_3](t) = a\left(1 - e^{-k_b t}\right). \qquad (4)$$

Having accounted for the methane molecules and methyl radical, we would like to comment on the possible formation pathways of the remaining molecules formed during the electron exposure as listed in Table 2. The proposed reaction sequence is shown in Figure 5. The system of coupled differential equations was solved numerically (Frenklach et al. 1992). The underlying rate constants found for each process are compiled in Table 5 and the resulting kinetic fits to the column densities of each species are shown in Figure 6. In this scheme it was assumed that the generation of the internally excited ethane molecules obeyed pseudo–first-order kinetics, the rate constant, k_1,

was found to be 6.14×10^{-5} s^{-1}. This value is about an order of magnitude less than the formation of the methyl radicals via equation (4), suggesting that most of the methyl radicals generated via homolytic carbon-hydrogen bond rupture processes do not have the proper reaction geometry to recombine and/or are not located in the same matrix cage. The internally excited ethane molecule can either be stabilized via phonon interaction (transferring the internal energy to the matrix; reaction [5], k_2) or can undergo unimolecular decomposition via atomic (k_3) and/or molecular (k_4) hydrogen elimination (reactions [6] and [7]; Fig. 5). Note that the energetics for reactions (6) and (7) are analogous to reactions (R6) and (R7) in Table 4. Here, we derived rate constants of $k_2 = 2.09 \times 10^{-2}$ s^{-1}, $k_3 = 5.52 \times 10^{-3}$ s^{-1}, and $k_4 = 3.18 \times 10^{-3}$ s^{-1}.

$$[\text{C}_2\text{H}_6]^* \rightarrow \text{C}_2\text{H}_6(X\,^1A_{1g}), \qquad (5)$$

$$[\text{C}_2\text{H}_6]^* \rightarrow \text{C}_2\text{H}_5(X\,^2A') + \text{H}(^2S_{1/2}), \qquad (6)$$

$$[\text{C}_2\text{H}_6]^* \rightarrow \text{C}_2\text{H}_4(X\,^1A_g) + \text{H}_2(X\,^1\Sigma_g^+)/2\text{H}(^2S_{1/2}). \qquad (7)$$
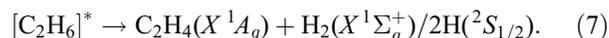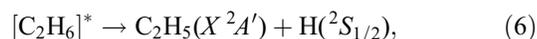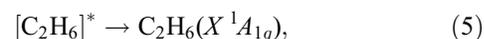
Thus, we can conclude that the majority (∼70%) of the excited ethane molecules can be stabilized by the surrounding matrix to form the ground state ethane molecule via reaction (5). However, the fact that both k_3 and k_4 were found to be nonzero, means that these pathways are also significant. If we assume that ethane is formed via the recombination of methyl radicals via reaction (R5), there is an excess of 3.74 eV from this process. However, for reaction (6) to proceed it would require 4.27 eV (an additional 0.53 eV), which means that a considerable number of the methyl radicals formed via reaction (R1) must hold excess energy of at least 0.26 eV each. Similarly, in reaction (7) the elimination of molecular hydrogen from the excited ethane molecule has a barrier of 4.58 eV (an additional 0.84 eV), meaning that a significant population of the methyl radicals formed under reaction (R1) are internally excited by at least 0.42 eV.

The formation of the ethyl radical appears to involve two pathways, k_3(reaction [6]), which has already been discussed, and its formation via the radiolysis of a previously formed ground state ethane molecule (reaction [R6]). Here, the rate constant, k_5, was found to be 3.12×10^{-3} s^{-1}. The fact that k_5 is slower than k_3 and, in addition, is also dependant on k_2 means that the majority

TABLE 4

Summary of the Reactions Involved in this Study

Reaction No.	Reaction	$\Delta_R G$		ΔE_b	
		kJ mol^{-1}	eV	kJ mol^{-1}	eV
R1....................	$CH_4(X^1A_1) \rightarrow CH_3(X^2A_2'') + H(^2S_{1/2})$	427.5[a]	4.43[a]	...	...
		432.4[b]	4.48[b]		
R2....................	$H(^2S_{1/2}) + H(^2S_{1/2}) \rightarrow H_2(X^1\Sigma_g^+)$	218[b]	2.26[b]	...	...
R3....................	$CH_4(X^1A_1) \rightarrow CH_2(a^1A_1) + H_2(X^1\Sigma_g^+)$	456.6[b]	4.73[b]	...	...
R4....................	$CH_4(X^1A_1) \rightarrow CH(X^2\Pi) + H_2(X^1\Sigma_g^+) + H(^2S_{1/2})$	876.7[b]	9.08[b]	...	...
R5....................	$CH_3(X^2A_2'') + CH_3(X^2A_2'') \rightarrow [C_2H_6]^*$	−360.7[a]	−3.74[a]	...	...
R6....................	$C_2H_6(X^1A_{1g}) \rightarrow C_2H_5(X^2A') + H(^2S_{1/2})$	411.7[a]	4.27[a]	...	...
R7....................	$C_2H_6(X^1A_{1g}) \rightarrow C_2H_4(X^1A_g) + H_2(X^1\Sigma_g^+)/2H(^2S_{1/2})$	−131.8[c]	−1.37[c]	477[c]	4.94[c]
				442[c]	4.58[c]
R8....................	$C_2H_5(X^2A') \rightarrow C_2H_4(X^1A_g) + H(^2S_{1/2})$	148[a]	1.53[a]	157[a]	1.62[a]
R9....................	$C_2H_6(X^1A_{1g}) \rightarrow C_2H_3(X^2A') + H(^2S_{1/2}) + H_2(X^1\Sigma_g^+)$	584.2[b]	6.05[b]	?	?
R10..................	$C_2H_5(X^2A') \rightarrow C_2H_3(X^2A') + H_2(X^1\Sigma_g^+)$	not accessible[d]	not accessible[d]	?[d]	?[d]
R11..................	$C_2H_4(X^1A_g) \rightarrow C_2H_3(X^2A') + H(^2S_{1/2})$	452.4[a]	4.69[a]	...	...
R12..................	$C_2H_4(X^1A_g) \rightarrow C_2H_2(X^1\Sigma_g^+) + H_2(X^1\Sigma_g^+)/2H(^2S_{1/2})$	154.8[e]	1.60[e]	524[e]	5.43[e]
				458[e]	4.75[e]
				392[e]	4.06[e]
R13..................	$C_2H_3(X^2A') \rightarrow C_2H_2(X^1\Sigma_g^+) + H(^2S_{1/2})$	147[a]	1.52[a]	163[a]	1.69[a]
R14..................	$H(^2S_{1/2}) + CH_4(X^1A_1) \rightarrow CH_3(X^2A_2'') + H_2(X^1\Sigma_g^+)$	0.28[f]	0.003[f]	62.46[f]	0.65[f]
R15..................	$H(^2S_{1/2}) + C_2H_6(X^1A_{1g}) \rightarrow C_2H_5(X^2A') + H_2(X^1\Sigma_g^+)$	−29.2[g]	−0.3[g]	50.2[g]	0.52[g]
R16..................	$H(^2S_{1/2}) + C_2H_5(X^2A') \rightarrow C_2H_4(X^1A_g) + H_2(X^1\Sigma_g^+)$	−273.5[h]	−2.8[h]	3.2[h]	0.03[h]
R17..................	$H(^2S_{1/2}) + C_2H_4(X^1A_g) \rightarrow C_2H_3(X^2A') + H_2(X^1\Sigma_g^+)$	24.7[i]	0.26[i]	63[i]	0.65[i]
R18..................	$H(^2S_{1/2}) + C_2H_3(X^2A') \rightarrow C_2H_2(X^1\Sigma_g^+) + H_2(X^1\Sigma_g^+)$	−280.97[j]	−2.91[j]	103.8[j]	1.08[j]

Notes.—The Gibbs free energy for the reaction ($\Delta_R G$) is given along with the energy of any additional barrier that may exist (ΔE_b). A question mark indicates that although a barrier likely exists, to our knowledge it has not been calculated.
[a] Calculated value (see Appendix).
[b] See http://webbook.nist.gov/chemistry.
[c] Value from Irle & Morokuma (2000).
[d] Value from Mebel et al. (1995).
[e] Value from Jensen et al. (1994).
[f] Value from Wu et al. (2004).
[g] Value from Kerkeni & Clary (2005).
[h] Value from Zhang et al. (2004).
[i] Value from Knyazev et al. (1996).
[j] Derived from triplet potential energy surface derived by Kim et al. (2003) which is 79.9 kJ mol^{-1} (0.83 eV) above the singlet ground state (Sherrill et al. 2000).
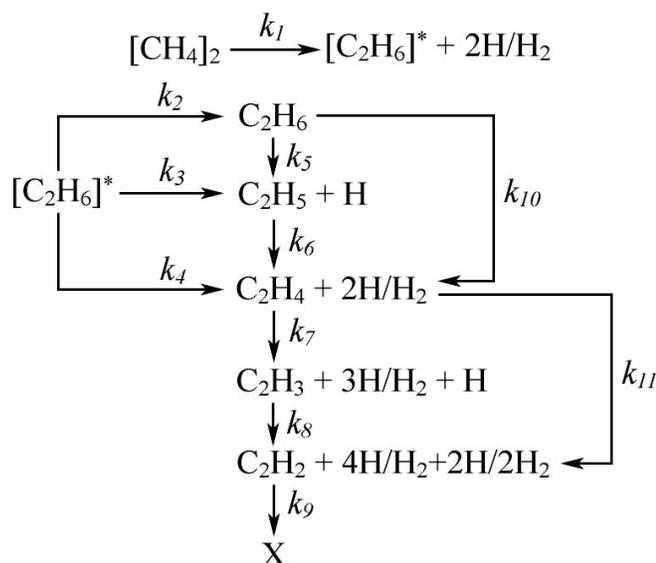
Fig. 5.—Reaction scheme used to fit the column densities of the C_2H_x species ($x = 2$–6) observed during the irradiation.

of the ethyl radical is produced via reaction (6), although reaction (R6) is still significant. In comparison of the destruction rates of the ethane and ethyl radicals through radiolysis to produce the ethyl radical (R6) and ethylene (R8), respectively, the latter was found to proceed faster, where k_6 was found to be 4.12×10^{-3} s^{-1}. The energetics can also explain this by the fact that the energy required to produce the ethyl radical through reaction (R6), 4.27 eV, is more than the energy required to produce the ethylene molecule through reaction (R8), 1.62 eV (including the barrier), i.e., the reaction requiring the least energy proceeds the fastest.

Now, let us compare the reaction rates of the formation of ethylene from ground state ethane molecules (k_{10}; reaction [R7]) and its formation through the decomposition of the internally excited ethane molecule (k_4; reaction [7]). The rate constant for reaction (R7), k_{10}, was found to be 2.28×10^{-6} s^{-1}, roughly 3 orders of magnitude smaller than k_4. Here, we find that the more important pathway to form ethylene appears to be through reaction (7), which implies that the molecular hydrogen elimination from a molecule of ethane is more likely to occur during the recombination of energetic methyl radicals. An investigation of the relevant energetics provides little insight into the reason for this discrepancy, as both reaction (R7) and reaction (7) infer the elimination of a molecule of hydrogen from ethane. However, the theoretical investigation by Irle & Morokuma (2000) reported two different possible reaction pathways for this process, either both hydrogens being eliminated from different carbon
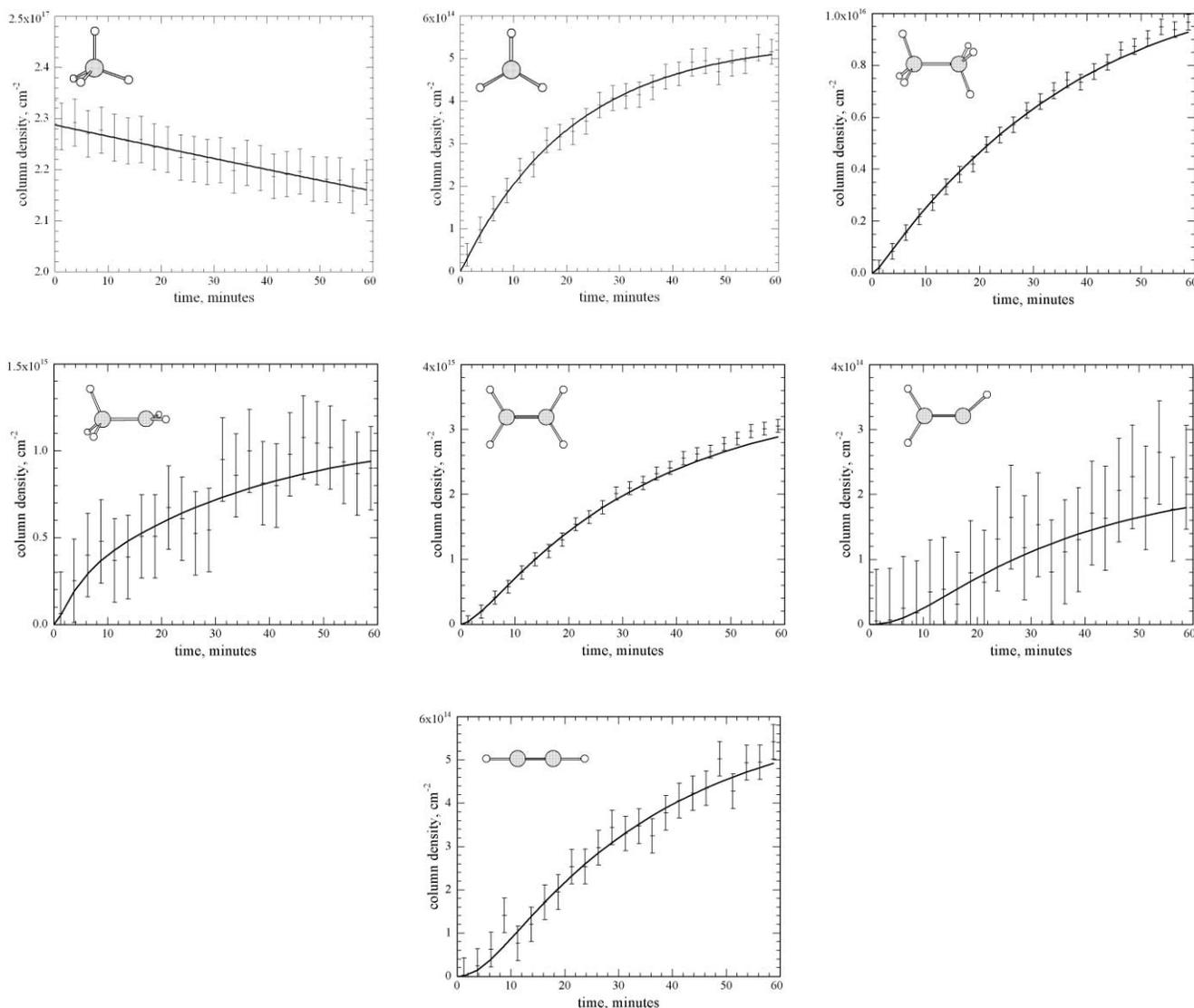
Fig. 6.—Fit of the column densities of methane (*top left*), methyl, (*top center*) ethane (*top right*), ethyl (*center left*), ethylene (*center*), vinyl (*center right*), and (*bottom*) acetylene.

atoms (barrier of 4.94 eV) or the hydrogens being eliminated from the same carbon atom (barrier of only 4.58 eV). In addition, the competing pathway to the formation of the ethyl radical via reactions (R6) and (6) lies only 4.27 eV above the ground state of the ethane molecule. The formation of ethylene through the dissociation of the ethyl radical (k_6; reaction [R8]) also contributes a significant amount to the formation of the ethylene molecule.

In agreement with the theoretical calculations carried out by Mebel et al. (1995), no rate constant could be found for reaction (R10), the elimination of molecular hydrogen to form the vinyl radical from the ethyl radical. In fact, the only formation pathway that was found for the production of the vinyl radical was the radiolysis-induced hydrogen elimination of the ethylene molecule, reaction (R11). The rate constant for this reaction, k_7, was found to be 2.31×10^{-4} s^{-1}. The destruction of the vinyl radical was found to proceed via the radiolysis-induced hydrogen elimination reaction of the vinyl radical to form the acetylene molecule, reaction (R13). Here, the rate constant, k_8, was found to be 3.56×10^{-3} s^{-1}. Once again, the destruction rates for radicals appear to be faster than those for the closed-shell species, reflected by the relative required energy for the hydrogen elimination

TABLE 5
Rate Constants Derived via Iterative Solution
to the Reaction Scheme Depicted in Fig. 5

Reaction	Rate Constant (s^{-1})
$[CH_4 \ldots CH_4] \rightarrow C_2H_6^* + 2H/H_2$	$k_1 = 6.14 \times 10^{-5}$
$C_2H_6^* \rightarrow C_2H_6$	$k_2 = 2.09 \times 10^{-2}$
$C_2H_6^* \rightarrow C_2H_5 + H$	$k_3 = 5.52 \times 10^{-3}$
$C_2H_6^* \rightarrow C_2H_4 + 2H/H_2$	$k_4 = 3.18 \times 10^{-3}$
$C_2H_6 \rightarrow C_2H_5 + H$	$k_5 = 3.12 \times 10^{-3}$
$C_2H_5 \rightarrow C_2H_4 + H$	$k_6 = 4.12 \times 10^{-3}$
$C_2H_4 \rightarrow C_2H_3 + H$	$k_7 = 2.31 \times 10^{-4}$
$C_2H_3 \rightarrow C_2H_2 + H$	$k_8 = 3.56 \times 10^{-3}$
$C_2H_2 \rightarrow X$	$k_9 = 8.33 \times 10^{-3}$
$C_2H_6 \rightarrow C_2H_4 + 2H/H_2$	$k_{10} = 2.28 \times 10^{-6}$
$C_2H_4 \rightarrow C_2H_2 + 2H/H_2$	$k_{11} = 1.22 \times 10^{-3}$

TABLE 6

Column Densities of Species at the End of Irradiation and the Number of Molecules Produced per Incident Electron

Species	Molecules Produced (molecules cm^{-2})	Number of Molecules Produced per Electron	Minimum Energy per Molecule (eV)	Total Energy Translated to Matrix per Electron (eV)	Carbon Atoms Produced (cm^{-2})
CH$_4$	$(-1.15 \pm 0.63) \times 10^{16}$	-11.7 ± 6.4	4.42	-52 ± 28	$(-1.15 \pm 0.63) \times 10^{16}$
CH$_3$	$(5.16 \pm 0.30) \times 10^{14}$	0.52 ± 0.03	4.42	2.32 ± 0.13	$(5.16 \pm 0.30) \times 10^{14}$
C$_2$H$_6$	$(9.66 \pm 0.24) \times 10^{15}$	9.82 ± 0.24	8.84	87 ± 2^a	$(1.93 \pm 0.05) \times 10^{16}$
C$_2$H$_5$	$(9.0 \pm 1.5) \times 10^{14}$	0.91 ± 0.15	13.11	12 ± 2	$(1.80 \pm 0.30) \times 10^{15}$
C$_2$H$_4$	$(3.05 \pm 0.10) \times 10^{15}$	3.10 ± 0.10	14.74	45.7 ± 1.5^b	$(6.11 \pm 0.19) \times 10^{15}$
C$_2$H$_3$	$(2.3 \pm 0.8) \times 10^{14}$	0.23 ± 0.08	19.43	4 ± 2	$(4.53 \pm 1.62) \times 10^{14}$
C$_2$H$_2$	$(5.24 \pm 0.41) \times 10^{14}$	0.53 ± 0.04	21.1	11 ± 1	$(1.05 \pm 0.08) \times 10^{15}$
Total^c				163 ± 4	$(2.93 \pm 0.06) \times 10^{16}$

Notes.—The minimum energy required to produce one molecule of each species is listed, combined with the total energy which must be translated to the matrix per impinging electron. Also listed is the number of carbon atoms within the reported column densities.

^{a} During warm-up, the column density increases to around 2.8×10^{16} molecules cm^{-2}; requiring approximately 252 eV to be translated to the matrix per 5 keV electron implanted.

^{b} On heating, the column density was found to increase to a value of $5.9 \pm 0.2 \times 10^{15}$ molecules cm^{-2}, which would require 88 ± 3 eV transferred to the sample per electron implant.

^{c} The total values listed here do not include the energy required to destroy methane as it is already accounted for in the production of the products.

processes being 4.69 eV for elimination from ethylene through reaction (R11), and 1.69 eV for elimination from the vinyl radical via reaction (R13). A second formation pathway to acetylene via the elimination of molecular hydrogen from ethylene was also found (reaction [R12]). Here, the rate constant, k_{11}, was found to be 1.22×10^{-3} s^{-1}, which although slower than k_8, does not depend on the prior formation of the vinyl radical from ethylene, which was actually found to be *slower* ($k_7 = 2.31 \times 10^{-4}$ s^{-1}) than the direct formation of acetylene via reaction (R12). The minimum energy pathway established by Jensen et al. (1994) for the elimination of molecular hydrogen from ethylene was found to have a barrier at 4.06 eV above the ethylene molecule in its ground state. Whereas the energy required for hydrogen elimination from ethylene into the vinyl radical was found to require 4.69 eV, which might help explain why this reaction occurs more slowly. In summary, the dominant pathway for the production of acetylene appears to be through the elimination of molecular hydrogen from ethylene, possibly via the CH$_3$CH intermediate tentatively identified in our experiment (or H$_2$CC). Lastly, to account for further reactions of the acetylene molecule a final reaction pathway was included,

$$C_2H_2(X\,^1\Sigma_g^+) \rightarrow X, \tag{8}$$
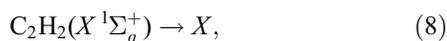
where X represents any further hydrocarbon not covered by this study that acetylene might react to form (e.g., polymerization). The rate constant for this reaction, k_9, was found to be 8.33×10^{-3} s^{-1}.

It should be noted that the reaction scheme presented here is not complete, in that there are several possible alternative pathways for the formation of these species that have been omitted, as it is not currently possible to distinguish them from the pathways that have been covered. Reactions (R14)–(R18) in Table 4 show possible alternative pathways to forming these molecules involving suprathermal (nonequilibrium) hydrogen atoms. These can be generated through reaction (R1) and, due to the exothermicity of this reaction, will bear excess kinetic energy and be mobile within the lattice. These suprathermal hydrogen atoms can then undergo hydrogen abstraction reactions, which are very favorable, as indicated by their exothermicity, due to the formation of molecular hydrogen. For example, a hydrogen abstraction pathway could be partially responsible for generating the ethyl radical via reaction (R15). This reaction is exoergic by 29.2 kJ mol^{-1} (0.3 eV) and has been stud-

ied by Kerkeni & Clary (2005), who found the reaction has a barrier of 50.2 kJ mol^{-1} (0.52 eV), which must be provided by the suprathermal hydrogen atom but is much lower than the barrier to required by competing reactions (R6) and (6). Please refer to reactions (R14)–(R18) and the references listed in Table 4 for more information on how hydrogen abstraction reactions may be candidate reaction pathways for generating each of the other species covered in this study.

4.2. Energetics

Let us now consider how much energy is required to produce the observed column densities of the species observed in our experiment. Considering the destruction of methane itself, we can assume that the predominant reaction pathway is reaction (R1), the homolytic cleavage of the σ C—H bond, creating the methyl radical and a hydrogen atom, as the methylene (CH$_2$) and methylidyne (CH) radicals were not observed experimentally. The calculated energy for this reaction requires 426.7 kJ mol^{-1} (4.42 eV) compared to an experimental value of 432.4 kJ mol^{-1} (4.48 eV); all experimental reaction energies are derived from values published in the NIST Chemistry WebBook[4] unless stated otherwise; all calculated values stated were found via the CCSD(T)/aug-cc-pVTZ method described in § A1. Table 6 summarizes the numbers of each species produced or destroyed throughout the hour of irradiation with 5 keV electrons at 100 nA as well as how much of the electrons' kinetic energy is transferred into the matrix during this process. The energy required per molecule assumes the minimum energy pathway to produce each species via the reactions listed in Table 4. For example, accounting for the number of methane molecules destroyed per electron, 11.7 ± 6.4 molecules, and if the destruction of each molecule requires 4.42 eV, this translates to 52 ± 28 eV being transferred to the sample as each electron is transmitted through the sample (using our calculated values). Recall from § 2 that the CASINO calculations estimate 370 eV will be transferred to the sample per electron, thus accounting for the destruction of methane by reaction (R1) may account for around 14% of the transferred energy. From the column density of the methyl radical, however, each electron produces 0.52 ± 0.03 methyl radicals, which translates to only 2.32 ± 0.13 eV, indicating that if reaction (R1) is solely responsible for the destruction of methane, then the methyl radicals must react further. Note

that at 10 K the methyl radicals are predicted not to be mobile within the lattice (Zhitnikov & Dmitriev 2002). The hydrogen atoms, on the other hand, can diffuse even at temperatures as low as 10 K and can recombine to form molecular hydrogen,

$$H(^2S_{1/2}) + H(^2S_{1/2}) \rightarrow H_2(X\,^1\Sigma_g^+). \qquad (9)$$
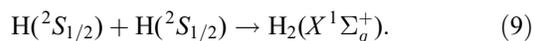
At 10 K even molecular hydrogen can diffuse in the matrix; once a hydrogen molecule reaches the surface, it can sublime into the gas phase. Molecular hydrogen was the only product identified by our mass spectrometer during the irradiation process.

The failed detection of either the methylene radical via

$$CH_4(X\,^1A_1) \rightarrow CH_2(a\,^1A_1) + H_2(X\,^1\Sigma_g^+) \qquad (10)$$
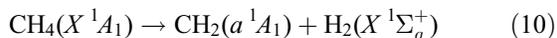
as well as the methylidyne radical through

$$CH_4(X\,^1A_1) \rightarrow CH(X\,^2\Pi) + H_2(X\,^1\Sigma_g^+) + H(^2S_{1/2}) \qquad (11)$$
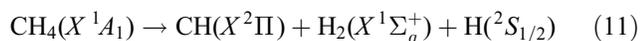
is found to be in contrast to photolysis experiments using UV photons. Here, a photolysis of pure methane at 1236 Å (10.03 eV) gives a quantum yield for the dissociation pathways in reaction (R1) and equations (10) and (11) of 0.44, 0.5, and 0.06, respectively (Okabe 1978). Note that recent experiments with low-energy electrons suggest that the cross section for the production of the methyl radical is larger than that for the formation of methylene by a factor of 20; while the maximum cross section for the generation of both radicals seems to lie where the energy of the impinging electron is around 20 eV (Nakano et al. 1991; Alman et al. 2000).

Considering the formation of ethane, $C_2H_6(X\,^1A_{1g})$, the most likely formation pathway is therefore the recombination of two neighboring methyl radicals of the proper reaction geometry within the same matrix cage. Since the recombination of two methyl radicals is calculated to be exoergic by 360.7 kJ mol^{-1} (3.74 eV), this process (reaction [R5]) leads to the formation of an internally excited molecule that can then relax (via phonon transfer to the lattice) to form the ground state ethane molecule (reaction [5]) or fragment via unimolecular decomposition (reactions [6] and [7]). To calculate the required energy to form ethane, we assume that it requires the formation of two methyl radicals via reaction (R1), each requiring 4.42 eV (8.84 eV total). No further energy is required to produce the ethane molecule as the combination of methyl radicals occurs exoergically and without barrier (reaction [R5]). Accounting for the observed column density of $9.66 \pm 0.24 \times 10^{15}$ ethane molecules cm^{-2} (9.82 ± 0.24 per electron) therefore requires a total energy of 87 ± 2 eV per implant (Table 6). Methyl radicals were also found to recombine during the warm-up phase to produce ethane (2.8×10^{16} molecules cm^{-2}); therefore, a total of 252 eV per 5 keV electron implant are needed to verify for the experimentally observed ethane column density energetically.

The ethyl radical can be generated by two similar processes that require differing energies and kinetics. The first pathway that we consider is the radiolysis-induced dissociation of a previously created ethane molecule to bear the ethyl radical and atomic hydrogen (reaction [R6]). The energy of this reaction was calculated to lie 411.7 kJ mol^{-1} (4.27 eV) above the energy of the ethane molecule. The second pathway supposes that the internally excited ethane molecule initially produced in reaction (6) immediately dissociates into the ethyl radical and a hydrogen atom. This reaction pathway requires that the methyl radicals bear enough kinetic energy when they recombine to overcome the additional energy requirements of this process (the recombination process is

only exoergic by 3.74 eV, whereas the reaction requires 4.27 eV, so an additional 0.53 eV is required). In order to calculate how much energy is deposited by the electron into the sample is required to account for the observed column density of the ethyl radical, we use the value from the pathway that requires the least energy; therefore, the energy required to form the ethyl radical can be calculated as the addition of this energy of that needed to form the ethane molecule (i.e., $4.27 + 8.84 = 13.11$ eV). To account for the column density after irradiation, $9.0 \pm 1.5 \times 10^{14}$ molecules cm^{-2} (0.91 ± 0.15 per electron) would therefore require 12 ± 2 eV transmitted to the sample per electron implant. A similar approach, based on the reactions listed in Table 4, was used to calculate the energy requirements to account for the observed column densities of the remaining species, the summary of which is shown in Table 6.

The total energy required to be transferred to the sample to account for all the observed products produced at the end of the 1 hr irradiation at 100 nA is 163 ± 4 eV per electron, or about 44% of the energy calculated to be transmitted to the sample using the CASINO code (see § 2).

4.3. Carbon Budget

To briefly address the issue of the carbon budget within the present experiment (i.e., can the column density of methane destroyed account for the column densities of the combined products; Table 6), we conclude that in total $1.15 \pm 0.63 \times 10^{16}$ methane molecules were destroyed per square centimeter. The total numbers of carbon atoms required to account for the observed column densities of the products at the end of irradiation are methyl radical $= 5.16 \pm 0.30 \times 10^{14}$, ethane $= 1.93 \pm 0.05 \times 10^{16}$, the ethyl radical $= 1.80 \pm 0.30 \times 10^{15}$, ethylene $= 6.11 \pm 0.19 \times 10^{15}$, the vinyl radical $= 4.53 \pm 1.62 \times 10^{14}$, and acetylene $= 1.05 \pm 0.08 \times 10^{15}$. The total number of carbon atoms required by the observed number of products is therefore $2.93 \pm 0.06 \times 10^{16}$ carbon atoms cm^{-2}, i.e., almost 3 times more than the amount of methane destroyed. How can we account for this discrepancy? The use of calculated absorption coefficients has an associated error of up to 20% compared to gas phase values, although for small hydrocarbons this value may lie closer to 5% (Galabov et al. 2002). In the solid state, it is well known that these absorption coefficients are distorted *for each band* associated with the molecule according to the chemical and physical conditions of the surrounding ice matrix, which will itself be altered during the irradiation process (Moore et al. 2001). It should also be noted that small contributions from other molecules not covered in this study may underlie some of the absorptions treated quantitatively. For example, the column density of ethane, which is based on the area of the band centered at 822 cm^{-1} (ν_{12} [CH$_3$ rock]) may be slightly lower than reported due to the overlapping band of another molecule even *within* this study, the weak absorption at around 820 cm^{-1} from ethylene (ν_{10} [CH$_2$ rock]).

4.4. Temporal Profiles

We would now like to comment on some of the conclusions that can be drawn from the temporal evolution of the column densities depicted in Figures 4a–4g. First, it is clear that the column densities of all species remain constant during the isothermal stage, where the ice is held for 1 hr at 10 K (within the limits of the error bars, with the possible exception of the vinyl radical; Fig. 4f). Once the temperature program is initiated, we see a gradual decrease in the column density of methane as it sublimes from the target (Fig. 4a). It is of little surprise that the column densities of the unstable radical species decrease sharply as

TABLE 7
COMPARISON OF QUANTITATIVE RESULTS FROM ELECTRON BOMBARDMENT

IRRADIATION SOURCE	DOSE (eV molecule^{-1})	COLUMN DENSITIES (molecules cm^{-2})						REFERENCE
		[CH$_4$] Initial ($\times 10^{17}$)	[CH$_4$] Destroyed ($\times 10^{16}$)	[CH$_3$] Produced ($\times 10^{14}$)	[C$_2$H$_6$] Produced ($\times 10^{15}$)	[C$_2$H$_4$] Produced ($\times 10^{15}$)	[C$_2$H$_2$] Produced ($\times 10^{15}$)	
5 keV electrons	1.6 ± 0.2	2.29 ± 0.05	1.15 ± 0.63	5.16 ± 0.30	9.66 ± 0.24	3.05 ± 0.10	0.52 ± 0.04	1
UV photons..................	7.2	7.2	46.4	0.98[a]	5.0	7.0	NA[b]	2
	~135	1.30*	9.2*	NA	8.58*	NA	NA	3
30 keV protons	~105	1.60*	15*	NA	2.8*[c]	NA	NA	3
7.3 MeV protons...........	28 ± 3	78.1 ± 0.8	69.8	1276	1339*	248	144.3	4
9.0 MeV α-particles......	29 ± 2	85.7 ± 1.0	140	2020	2048*	482	265.8	4

NOTES.—Bombardment is with 5 keV electrons at 0.1 μA for 1 hr with those from previous experiments using UV photolysis and ion irradiation. The irradiation source is stated (refer to the individual papers for more details), the dose used, the column densities of methane before and after irradiation, as well as the final column densities of the methyl radical, ethane, ethylene and acetylene. NA indicates that the column density of this species was not presented. An asterisk (*) indicates value may not be reliable for comparison as different absorption bands were used to calculated the column densities of these molecules
[a] Value at the end of irradiation. A maximum column density of 4.4×10^{14} molecules cm^{-2} was found at a dose of 0.36 eV molecule^{-1}.
[b] Although no quantitative results were presented, absorptions corresponding to the two strongest peaks were present.
[c] Value at the end of irradiation. A maximum column density of 1.32×10^{16} molecules cm^{-2} was found at a dose of 23 eV molecule^{-1}.
REFERENCES.—(1) This work; (2) Gerakines et al. 1996; (3) Baratta et al. 2002; (4) Kaiser & Roessler 1998.

soon as the temperature begins to increase for the methyl (Fig. 4*b*), ethyl (Fig. 4*d*), and vinyl (Fig. 4*f*) radicals. It could be expected that the column densities of the closed shell species should, however, be relatively unaffected by the slight increase in temperature, as can be seen by the increase in column densities of both the ethane molecule (Fig. 4*c*) and the ethylene molecule (Fig. 4*e*). However, the column density of acetylene (Fig. 4*g*) also appears to decrease immediately as the temperature is increased. The slight increase in column density of the ethane molecule can likely be accounted for by the increased mobility of the methyl radicals, which can then recombine to form ethane via reactions (R5) and (5). The increase in the column density of ethylene cannot be explained in a similar manner, as no evidence of the methylene radicals was found. One possible explanation is the recombination of hydrogen atoms trapped within the lattice with the vinyl radical, which can without barrier form ethylene. Similarly free hydrogen atoms could also react with the ethyl radical to produce more ethane. An alternative production route for the generation of ethylene is reaction (R16), where the mobile hydrogen atoms abstract a hydrogen from the ethyl radical to generate ethylene and molecular hydrogen, which requires the hydrogen atoms to overcome the 0.03 eV energy barrier (at this time, the hydrogen atoms will be in thermal equilibrium with the surrounding matrix; therefore, less than 0.1% of the hydrogen atoms would be able to overcome this barrier, ignoring the possibility of tunneling). The simplest explanation for the disappearance of acetylene on warmup would be the hydrogenation to form the vinyl radical (reverse of reaction [R13]; Fig. 9, *bottom*) which could also be subsequently hydrogenated to form more ethylene. However, recall that this would need to overcome an energy barrier of 0.17 eV; at below 40 K, the population of hydrogen atoms that have this energy would not be significant. It is therefore likely that the majority of reactions involving the acetylene molecule during the heating period produce higher hydrocarbons not covered in this study. It is also likely that the radical-radical recombination reactions of the methyl, ethyl, and vinyl radicals will produce higher hydrocarbons. Once the methane matrix has sublimed (39–42 K), a sharp increase in the column density of both the ethane and ethylene molecules is observed. This increase cannot be explained by reactions occurring involving any species covered within this study within the matrix as at this time, as their column densities indicate that they are no longer present within the matrix. The most likely explanation is that the intensities of the infrared absorptions

of the fundamentals used to calculate the column densities are stronger in the new matrix.

4.5. *Comparison to Previous Experiments*

We now would like to compare quantitatively, the results of electron bombardment on pure methane ices with those from experiments using UV photons and high-energy ions as the source of irradiation. Table 7 summarizes experiments where quantitative information regarding the destruction of methane and production of new molecules was presented. Note that in making a quantitative comparison, other experimental parameters such as the thickness of the sample and dose must be taken into consideration also.

First, regarding the destruction of methane over the course of the experiment, comparing the column density of methane before and after the experiment, we can conclude that roughly 5% of the total methane in our sample was destroyed throughout the irradiation process. In the experiments where UV photons were the source, note that in both cases most of the original methane in the sample was destroyed. In the experiments carried out by Gerakines et al. (1996) they exposed the sample to a dose of 7.2 eV molecule^{-1}, resulting in roughly 65% of the methane being destroyed. Note that the additional 128 eV molecule^{-1} used in experiments by Baratta et al. (2002), caused the destruction of only an additional 5% to the sample. The authors reported on this discrepancy being due to the fact that during the irradiation process, the optical properties of the ice sample are modified. Initially however, the UV photons appear more efficient at destroying methane per eV molecule^{-1} absorbed in the sample. In the experiments with 30 keV protons by Baratta et al. (2002), the reported destruction of methane was much higher, at around 94% of the sample. This is a much greater percentage than the values obtained from Kaiser & Roessler (1998), where values were reported of around 9% for 7.3 MeV protons and 16% for 9.0 MeV α-particles. Before comparing the results of these experiments to those from our electrons, let us first check that they are internally consistent. The linear energy transfer for the electronic and nuclear processes for high-energy protons and α-particles impinging into our methane target was calculated using the Stopping and Range of Ions in Matter (SRIM) code of Zeigler et al. (1985); the results were calculated for a proton of energy 1 eV to 10 GeV (the results are in accordance with those published previously, e.g., Johnson 1990). For high-energy ions the energy transfer to the ice occurs almost

exclusively through electronic energy transfer processes. For a 7.3 MeV proton, the linear energy transfer through electronic interactions was calculated to be 3.9 keV μm^{-1} and considerably higher for a 9.0 MeV α-particle at 40.5 keV μm^{-1}, explaining why much more chemical processing was found in the case of α-particle bombardment compared to that from protons. Considering why the 30 keV protons seems more effective at processing the methane sample than the 7.3 MeV protons, the energy transfer through electronic loss processes of the 30 keV proton is calculated to be around 67.8 keV μm^{-1}, but additionally, nuclear interaction processes begin to become more important, contributing an additional 0.3 keV μm^{-1}. This explains why, in general, the chemical processing from a keV ion is greater than that for a MeV ion; note also that the nuclear interactions will introduce a different chemistry into the ice than electronic processes alone (Kaiser & Roessler 1998). Taking into account the number of methane molecules destroyed per eV molecule^{-1} put into the system, we can conclude that 5 keV electrons are more efficient at processing the methane sample than both of the ion sources used. This should not be surprising if we consider the electronic energy loss processes from a MeV ion into the ice will be used to generate δ electrons, which are responsible for processing the ice further (Kaiser & Roessler 1998).

Considering the generation of the methyl radical, the column density at the end of the irradiation accounted for around 0.23% of the methane destroyed. This value is much larger than the value obtained from Gerakines et al. (1996), who reported only 0.01% of the methyl radical accounted for with the products produced by the destruction of methane. Even at the highest column densities reported during the experiment, this still accounts for only 0.06% of the methane. This means that either the photons are less efficient at producing the methyl radical or the sample was possibly heated enough during the course of the experiment for the radicals to be mobile enough to recombine to form ethane more efficiently. Both of the high-energy ion implantation experiments by Kaiser & Roessler (1998) produced enough of the methyl radical to account for roughly 1%–2% of the methane destroyed. However, taking into account the dosage, we can conclude that the electrons and ions are roughly the same efficiency at producing the methyl radical.

We now consider the relative formation of ethane, ethylene, and acetylene in each system (due to the inconsistencies in the carbon budget previously mentioned, column densities are used here). With regards to our system, the column density of ethane, ethylene, and acetylene at the end of irradiation is $9.66 \pm 0.24 \times 10^{15}$, $3.05 \pm 0.10 \times 10^{15}$, and $5.24 \pm 0.41 \times 10^{14}$ molecules cm^{-2}, respectively. The only other experiment where all three molecules were accounted for quantitatively is the work from Kaiser & Roessler (1998), where the column densities from proton irradiation were 1.34×10^{18}, 2.48×10^{17}, and 1.44×10^{17} molecules cm^{-2} for ethane, ethylene, and acetylene, respectively. In addition, for the α-particles the column densities reported were 2.05×10^{18}, 4.82×10^{17}, and 2.66×10^{17} molecules cm^{-2} for ethane, ethylene, and acetylene, respectively. In each of these experiments, the relative trend holds that more ethane is produced than ethylene, and more ethylene is produced than acetylene, consistent with the view that the formation of acetylene is dependant on a prior formation of ethylene, which itself is dependant on the prior formation of ethane. The comparison to the keV ion bombardment experiments is a little trickier, as it is evident from the temporal profile that the ethane was also highly processed in the sample; however, taking the value from the maximum column density reported of 1.32×10^{16} molecules cm^{-2} at a dosage of 23 eV molecule^{-1}, we can conclude that the efficiency of

generating ethane is a little lower than for the MeV particles, which themselves are less efficient than electrons.

Unfortunately, neither experiment studying the effects of UV irradiation included the acetylene molecule in their study. However, in the UV experiments carried out by Gerakines et al. (1996), the ethane and ethylene can account for 2.2% and 3.0% of the methane destroyed, respectively. Here, we can note that overall, the efficiency of producing these molecules is far less than both irradiation by electrons and ions. Another surprising observation is that the ethylene molecule seems to be produced more efficiently than the ethane molecule within this system. This could be an anomaly due to the fact that possibly more of the ethane is processed to form the ethylene molecule. Alternatively, if ethylene really is produced more efficiently than ethane in this system, then we must be able to account for it somehow. One possible reason is that the UV photolysis generates methylene radicals with greater efficiency than the methyl radical (Okabe 1978). Both experiments seem less efficient at producing the ethane molecule.

In summary, it would appear at first that the electrons are the most efficient at forming new molecules with regards to the amount of products formed versus methane destroyed per eV per molecule. However, from the initial production rates of ethane via UV photolysis, it seems that this process may be more efficient, but it does not penetrate very far through the ice. The surface layers, however, are further processed, generating very small quantities of a wide range of species. In the case of radiolysis by electrons and ions, the carbon budget could not be conserved. However, when UV photolysis is used as the irradiation source, the early irradiation products covered by this study could only account for 5.2% of the methane destroyed.

5. ASTROPHYSICAL IMPLICATIONS

The polar ice grains within interstellar clouds are subject to irradiation from MeV ions and are expected to undergo similar chemical processes as in our experiment. It has been shown that when an MeV ion is implanted into an ice, more than 99.9% of the energy transferred is lost through electronic energy transfer processes, i.e., the generation of δ electrons, which then further process the ice (Kaiser & Roessler 1998). Thus, it is expected that the products from this irradiation experiment should be found within interstellar ices. A quantitative estimate to the abundance is difficult at this time, as little information exists on the abundance of neighboring methane molecules within these grains and also the effects of other matrix components (e.g., water) on the production rates of these species. Where the abundance of methane is only 1%–4%, the abundance of ethane is likely to be less than 1% and hitherto unlikely to be detected. However, in sources where the methane abundance is considerable, such as Mon R2 IRS 3 and GCS 4 the detection of these molecular species may be possible. Note that in a recent survey of low-mass protostars using the *Spitzer Space Telescope*, Boogert et al. (2004) mentioned two unidentified bands found in each source studied, located at 3.47 μm ($\sim$2880 cm^{-1}) and 6.85 μm ($\sim$1460 cm^{-1}), which happen to correspond to two absorptions from ethane, although ethane may be only one of several contributing species to the 3.47 μm feature.

As comets are thought to preserve the pristine interstellar material of the interstellar cloud from which our solar system was born, the molecules found within them is expected to be similar to the molecules produced in interstellar ices. Infrared studies on the volatile components from Oort cloud comets report the detection of methane, ethane, and acetylene (Mumma et al. 2003). The failed detection of ethylene within these comets possibly points to the fact that both ion and UV irradiation is not effective

at producing high abundances of ethylene within interstellar ices. This seems to be in contradiction to present theory, particularly in the case of UV photons, which has been demonstrated in laboratory experiments to produce higher abundances of ethylene than ethane. While possible gas-phase ion-molecule pathways to acetylene exist, the fact that in general a higher abundance is observed in warm clouds than cold clouds suggests that acetylene may be released during the sublimation of icy grain mantles as a young protostar develops (Boudin et al. 1998). It has also been suggested that there are other, possibly more efficient methods to generate acetylene within interstellar ices, via the successive hydrogenation of C_2 which is thought to be very efficient due to hydrogen migration and tunneling reactions within interstellar ices, so much in fact that it has been included as a pathway to form not only acetylene, but even ethane in models of intermolecular clouds (Hasegawa & Herbst 1993). Comets residing in the Oort cloud are chemically processed, predominantly by energetic ions from the Galactic cosmic radiation, over periods of around 10^9 yr. This is believed to produce an irradiation-driven mantle or crust around a meter thick, which may be able to explain why a comet can bear regions of inactivity as a comet enters the solar system. This crust is believed to consist of many chain molecules, with a high abundance of carbon and can be effectively reproduced in laboratory irradiation experiments of ices containing methane, even in the presence of water (Strazzulla & Johnson 1991; Kaiser & Roessler 1998).

These studies could also aid in the identification of hydrocarbons on solar system bodies. Coustenis et al. (2003) have analyzed the atmosphere of Saturn's moon Titan using *ISO* and found that not only are methane, ethane, ethylene, and acetylene present, but also more complex hydrocarbons such as propane, propyne, benzene, allene, and diacetylene. Most modeling of Titan is focused on attempting to recreate these molecules from gas-phase processes initiated by UV irradiation (e.g., Tran et al. 2005); however, it is clear that the surface is known to be bombarded by energetic ions, photons and electrons that are capable of producing more complex molecules in the solid state. A proportion of these may well be released into the gas phase and need to be incorporated into these models. High-energy electrons produced from Saturn's magnetosphere could be partly responsible for the production of these molecules (Cravens et al. 2005). Sasaki et al. (2005) recently conducted a search for nonmethane hydrocarbons on Pluto and found absorptions at 3.10, 3.22, and 3.35 μm (3225, 3125, and 2985 cm^{-1}), whereby the peak at 3.22 μm seems to be indicative of the presence of ethylene. Vernazza et al. (2005) reported the presence of features appearing at 3.42 μm (2920 cm^{-1}) and 3.06 μm (3268 cm^{-1}) on the surface of the asteroid 1 Ceres, which may be indicative of the presence of ethane and acetylene, respectively.

APPENDIX

A1. THEORETICAL CALCULATIONS

We have examined the structures and energetics of hydrocarbons of the C_2H_x ($x = 1-6$) series as well as the CH_y ($y = 1-4$) series, including different isomers and electronic states (where appropriate) in terms of ab initio molecular orbital methods employing the

TABLE 8
CALCULATED BAND POSITIONS AND INTEGRAL ABSORPTION COEFFICIENTS OF VARIOUS SPECIES SCALED BY 0.97

Band	Characterization	Band Position (cm^{-1})	A (cm molecule^{-1})
CH$_4(X\,^1A_1)$			
ν_1 (a_1).............................	CH symmetric stretch	2935	0
ν_2 (e)	CH bending	1514	1.66×10^{-19}
ν_3 (t).................................	CH asymmetric stretch	3037	4.65×10^{-18}
ν_4 (t).................................	CH bending	1302	2.82×10^{-18}
CH$_3(X\,^2A_2'')$			
ν_1 (a_1')	CH stretching	3011	0
ν_2 (a_2'')	Out-of-plane bend	491	1.39×10^{-17}
ν_3 (e')...............................	CH stretching	3185	1.16×10^{-18}
ν_4 (e')...............................	Deformation	1362	6.64×10^{-19}
CH$_2(X\,^3B_1)$			
ν_1 (a_1).............................	CH$_2$ symmetric stretch	3025	1.66×10^{-19}
ν_2 (a_1).............................	Bend	1024	1.99×10^{-18}
ν_3 (b_2).............................	CH$_2$ asymmetric stretch	3258	0
CH$_2(a\,^1A_1)$			
ν_1 (a_1).............................	CH$_2$ symmetric stretch	2797	1.53×10^{-17}
ν_2 (a_1).............................	Bend	1363	0
ν_3 (b_2).............................	CH$_2$ asymmetric stretch	2857	1.81×10^{-17}

TABLE 8—*Continued*

Band	Characterization	Band Position (cm^{-1})	A $(\text{cm molecule}^{-1})$
	$CH(X^2\Pi)$		
σ_g....................................	CH stretching	2720	2.92×10^{-17}
	$CH(a^4\Sigma^-)$		
σ_g....................................	CH stretching	2962	8.14×10^{-18}
	$C_2H_6(X^1A_{1g})$		
$\nu_1\ (a_{1g})$............................	CH_3 symmetric stretch	2935	0
$\nu_2\ (a_{1g})$............................	CH_3 symmetric deformation	1382	0
$\nu_3\ (a_{1g})$............................	CC stretch	967	0
$\nu_4\ (a_{1u})$............................	Torsion	298	0
$\nu_5\ (a_{2u})$............................	CH_3 symmetric stretch	2935	1.05×10^{-17}
$\nu_6\ (a_{2u})$............................	CH_3 symmetric deformation	1367	3.32×10^{-19}
$\nu_7\ (e_g)$............................	CH_3 degenerate stretch	2980	0
$\nu_8\ (e_g)$............................	CH_3 degenerate deformation	1459	0
$\nu_9\ (e_g)$............................	CH_3 rock	1182	0
$\nu_{10}\ (e_u)$............................	CH_3 degenerate stretch	3004	1.26×10^{-17}
$\nu_{11}\ (e_u)$............................	CH_3 degenerate deformation	1463	1.66×10^{-18}
$\nu_{12}\ (e_u)$............................	CH_3 rock	802	6.64×10^{-19}
	$C_2H_5(X^2A')$		
$\nu_1\ (a')$............................	CH_2 symmetric stretch	3045	2.82×10^{-18}
$\nu_2\ (a')$............................	CH_3 stretch	2944	4.65×10^{-18}
$\nu_3\ (a')$............................	CH_3 stretch	2855	5.15×10^{-18}
$\nu_4\ (a')$............................	CH_2 bend	1439	6.64×10^{-19}
$\nu_5\ (a')$............................	CH_2 bend	1421	3.32×10^{-19}
$\nu_6\ (a')$............................	CH_3 umbrella	1358	3.32×10^{-19}
$\nu_7\ (a')$............................	CC stretch	1030	0
$\nu_8\ (a')$............................	CH_3 rock	951	1.66×10^{-19}
$\nu_9\ (a')$............................	CH_2 out-of-plane	463	9.30×10^{-18}
$\nu_{10}\ (a'')$............................	CH_2 asymmetric stretch	3141	3.15×10^{-18}
$\nu_{11}\ (a'')$............................	CH_3 asymmetric stretch	2986	4.15×10^{-18}
$\nu_{12}\ (a'')$............................	CH_3 deformation	1439	9.96×10^{-19}
$\nu_{13}\ (a'')$............................	H deformation	1156	3.32×10^{-19}
$\nu_{14}\ (a'')$............................	H deformation	789	3.32×10^{-19}
$\nu_{15}\ (a'')$............................	Torsion	104	0
	$CH_2 = CH_2(X^1A_g)$		
$\nu_1\ (a_g)$............................	CH_2 symmetric stretch	3043	0
$\nu_2\ (a_g)$............................	CC stretch	1641	0
$\nu_3\ (a_g)$............................	CH_2 scissor	1339	0
$\nu_4(a_u)$................................	Torsion	1034	0
$\nu_5\ (b_{1g})$............................	CH_2 asymmetric stretch	3097	0
$\nu_6\ (b_{1g})$............................	CH_2 rock	1202	0
$\nu_7\ (b_{1u})$............................	CH_2 wag	945	1.66×10^{-17}
$\nu_8\ (b_{2g})$............................	CH_2 wag	944	0
$\nu_9\ (b_{2u})$............................	CH_2 asymmetric stretch	3124	5.15×10^{-18}
$\nu_{10}(b_{2u})$................................	CH_2 rock	810	1.66×10^{-19}
$\nu_{11}\ (b_{3u})$............................	CH_2 symmetric stretch	3028	3.15×10^{-18}
$\nu_{12}\ (b_{3u})$............................	CH_2 scissor	1428	1.49×10^{-18}
	$CH_3\text{-}CH(X^3A'')$		
$\nu_1\ (a')$............................	CH stretch	3110	1.16×10^{-18}
$\nu_2\ (a')$............................	CH stretch	2954	2.49×10^{-18}
$\nu_3\ (a')$............................	CH_3 symmetric stretch	2855	4.15×10^{-18}
$\nu_4\ (a')$............................	CH_3 deform	1410	1.16×10^{-18}
$\nu_5\ (a')$............................	CH_3 umbrella	1347	4.98×10^{-19}
$\nu_6\ (a')$............................	CC stretch	1068	0
$\nu_7\ (a')$............................	CH bend	1039	4.98×10^{-19}
$\nu_8\ (a')$............................	CH bend	738	2.16×10^{-18}

TABLE 8—*Continued*

Band	Characterization	Band Position (cm^{-1})	A $(cm\ molecule^{-1})$
$\nu_9\ (a'')$............................	CH_2 asymmetric stretch	2889	4.48×10^{-18}
$\nu_{10}\ (a'')$..........................	CH_3 deform	1410	1.16×10^{-18}
$\nu_{11}\ (a'')$..........................	CH_3 rock	964	3.32×10^{-19}
$\nu_{12}\ (a'')$..........................	Torsion	185	5.48×10^{-18}
	CH_3-$CH(a^1A)$		
$\nu_1\ (a)$..............................	CH stretch	2987	4.65×10^{-18}
$\nu_2\ (a)$..............................	CH_3 symmetric stretch	2897	8.97×10^{-18}
$\nu_3\ (a)$..............................	CH stretch	2815	1.66×10^{-17}
$\nu_4\ (a)$..............................	CH stretch	2745	1.83×10^{-18}
$\nu_5\ (a)$..............................	CH_2 scissor	1468	6.64×10^{-19}
$\nu_6\ (a)$..............................	CH_3 deform	1310	1.66×10^{-18}
$\nu_7\ (a)$..............................	CH_3 umbrella	1264	7.47×10^{-18}
$\nu_8\ (a)$..............................	CCH bend	1228	2.49×10^{-18}
$\nu_9\ (a)$..............................	CC stretch	1085	6.64×10^{-19}
$\nu_{10}\ (a)$............................	CH_2, CH bend	931	3.32×10^{-18}
$\nu_{11}\ (a)$............................	Twist	596	6.48×10^{-18}
$\nu_{12}\ (a)$............................	CH_3 wag	467	8.30×10^{-19}
	$CH_2 = CH(X^2A')$		
$\nu_1\ (a')$.............................	CH stretch	3139	1.66×10^{-19}
$\nu_2\ (a')$.............................	CH stretch	3040	9.96×10^{-19}
$\nu_3\ (a')$.............................	CH stretch	2947	9.96×10^{-19}
$\nu_4\ (a')$.............................	CC stretch	1601	3.32×10^{-19}
$\nu_5\ (a')$.............................	Bend	1349	1.49×10^{-18}
$\nu_6\ (a')$.............................	Rock	1015	1.66×10^{-18}
$\nu_7\ (a')$.............................	Bend	691	3.82×10^{-18}
$\nu_8\ (a'')$............................	Out-of-plane	893	1.30×10^{-17}
$\nu_9\ (a'')$............................	Torsion	795	2.99×10^{-18}
	CH_3-$C(X^2A'')$		
$\nu_1\ (a')$.............................	CH_3 asymmetric stretch	2875	3.82×10^{-18}
$\nu_2\ (a')$.............................	CH_3 symmetric stretch	2796	1.49×10^{-18}
$\nu_3\ (a')$.............................	CH_2 scissor	1401	1.33×10^{-18}
$\nu_4\ (a')$.............................	CH_3 umbrella	1269	1.28×10^{-17}
$\nu_5\ (a')$.............................	CC stretch	1063	2.32×10^{-18}
$\nu_6\ (a')$.............................	CH_3 wag	510	6.64×10^{-19}
$\nu_7\ (a'')$............................	CH_2 asymmetric stretch	2904	3.82×10^{-18}
$\nu_8\ (a'')$............................	CH_3 deform	1261	3.82×10^{-18}
$\nu_9\ (a'')$............................	CH_3 wag	826	0
	CH_3-$C(a^4A'')$		
$\nu_1\ (a')$.............................	CH_3 asymmetric stretch	2946	2.32×10^{-18}
$\nu_2\ (a')$.............................	CH_3 symmetric stretch	2881	3.65×10^{-18}
$\nu_3\ (a')$.............................	CH_2 scissor	1406	4.98×10^{-19}
$\nu_4\ (a')$.............................	CH_3 umbrella	1316	4.98×10^{-19}
$\nu_5\ (a')$.............................	CH_3 wag	980	1.66×10^{-18}
$\nu_6\ (a')$.............................	CC stretch	956	4.32×10^{-18}
$\nu_7\ (a'')$............................	CH_2 asymmetric stretch	2946	2.32×10^{-18}
$\nu_8\ (a'')$............................	CH_3 deform	1406	4.98×10^{-19}
$\nu_9\ (a'')$............................	CH_3 wag	980	1.66×10^{-18}
	$HCCH(X^1\Sigma_g^+)$		
$\nu_1\ (\sigma_g^+)$..........................	CH stretch	3418	0
$\nu_2\ (\sigma_g^+)$..........................	CC stretch	2008	0
$\nu_3\ (\sigma_u^+)$..........................	CH stretch	2930	1.46×10^{-17}
$\nu_4\ (\pi_u)$............................	CH bend	623	0
$\nu_5\ (\pi_u)$............................	CH bend	701	1.59×10^{-17}

TABLE 8—*Continued*

Band	Characterization	Band Position (cm^{-1})	A (cm molecule^{-1})
	H$_2$CC($X\,^1A_1$)		
ν_1 (a_1)...............................	CH$_2$ symmetric stretch	3021	7.31×10^{-18}
ν_2 (a_1)...............................	CC stretch	1659	1.43×10^{-17}
ν_3 (a_1)...............................	CH$_2$ scissor	1176	4.81×10^{-18}
ν_4 (b_1)...............................	Out-of-plane	728	1.49×10^{-17}
ν_5 (b_2)...............................	CH$_2$ asymmetric stretch	3097	3.15×10^{-18}
ν_6 (b_2)...............................	Rock	332	8.30×10^{-19}
	C$_2$H($X\,^2\Sigma^+$)		
ν_1 (σ^+)...............................	CH stretch	3357	9.13×10^{-18}
ν_2 (σ^+)...............................	CC stretch	2026	9.96×10^{-19}
ν_3 (π)...............................	Bend	360	3.32×10^{-19}

NOTES.—The vibrational band positions have been scaled by 0.97, to account for the anharmonicities; this factor is consistent with the B3LYP/6-311G(d,p) level of theory. The values of the band positions have been scaled by 0.97 to account for anharmonicity.

hybrid density functional B3LYP method (Lee et al. 1988; Becke 1993) with the 6-311G(d,p) basis functions in order to optimize the molecular structures at the energy minima (Fig. 2; Table 8). The relative energies were then refined by using the coupled cluster CCSD(T) method (Purvis & Bartlett 1982; Raghavachari et al. 1989) with the aug-cc-pVTZ basis functions (Dunning 1989) at the structures obtained by the B3LYP method. All relative energies were corrected by the zero-point vibrational energies calculated with
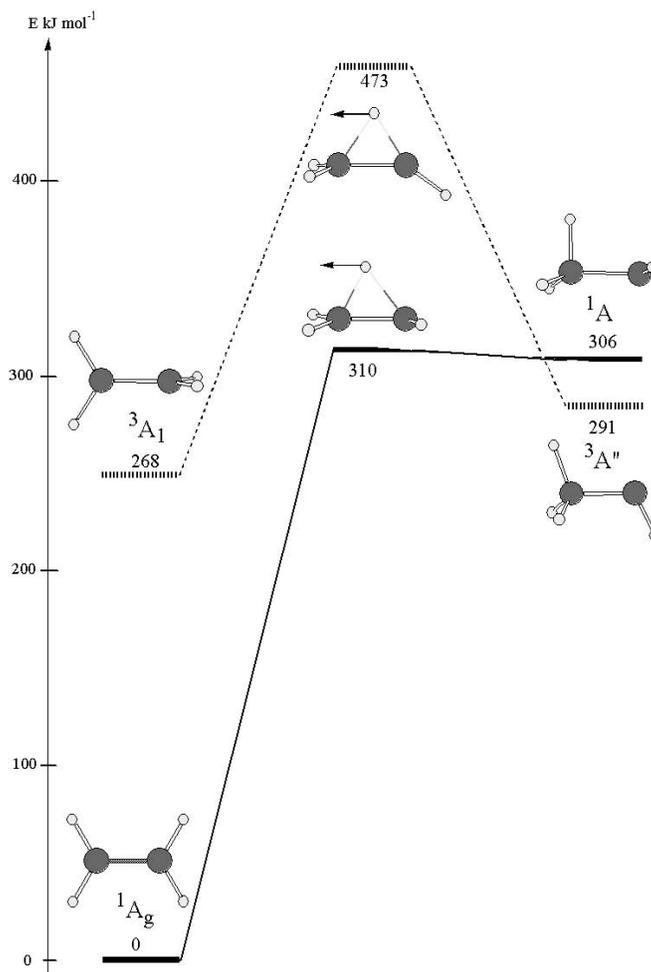
FIG. 7.—Potential energy surface of the isomerization between ethylene (C$_2$H$_4$) and methylcarbene (CHCH) in the ground and lowest excited triplet states calculated with B3LYP/6-311G(d,p) level of theory. The relative energies (in kilojoules per mole) were refined using the CCSD(T)/aug-cc-VTZ level of theory (see text for details). The solid line represents the potential energy surface of the ground state, and the dashed line indicates the potential energy surface of the lowest triplet state. [*See the electronic edition of the Journal for a color version of this figure.*]
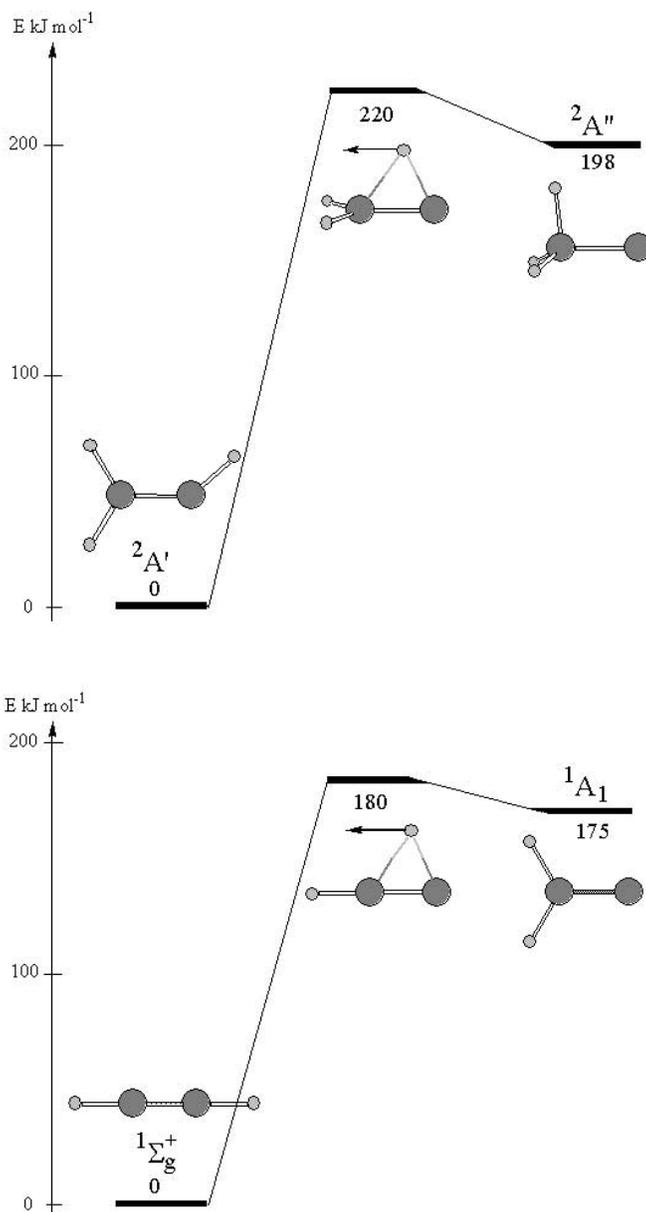
Fig. 8.—Potential energy surfaces of the hydrogen shift for the vinyl radical (C_2H_3; *top*) and acetylene (C_2H_2; *bottom*) calculated with the B3LYP/6-311G(d,p) level of theory. The relative energies (in kilojoule mole) were refined using the CCSD(T)/aug-cc-VTZ level of theory (see text for details). [*See the electronic edition of the Journal for a color version of this figure.*]

the B3LYP method without scaling. All calculations were carried out with the GAUSSIAN 98 program package (Frisch et al. 2001). In order to analyze the infrared spectra for the species obtained by present experiments, we have calculated the vibrational band position and infrared intensities for the structures obtained with the B3LYP/6-311G(d,p) method (Table 8). At this level of theory, the calculated intensities are typically accurate to about 20% (Galabov et al. 2002); however, experimentally derived solid-state intensities are used where possible.

A2. COMPUTATIONAL RESULTS

Figure 7 shows the potential energy surface of the isomerization between ethylene (C_2H_4) and methylcarbene (CH_3CH) in the ground and lowest excited triplet states calculated at the B3LYP/6-311(d,p) level of theory. On the ground state singlet surface, methylcarbene was found to be 306 kJ mol^{-1} higher in energy than ethylene; the barrier to isomerization is 310 kJ mol^{-1}, i.e., a barrier of only 4 kJ mol^{-1} for the reverse process. On the triplet surface, which exists 268 kJ mol^{-1} above the ground state, methylcarbene is only 23 kJ mol^{-1} less stable than twisted ethylene; the barrier to isomerism was computed to be 205 kJ mol^{-1}. Comparison of the triplet potential energy surface calculated by Kim et al. (2003) using the CCSD(T)/6-311+G(3df,2p) level of theory shows that the methylcarbene structure lies 24 kJ mol^{-1} above the ethylene structure, with a barrier of 208 kJ mol^{-1}. Figure 8 shows our potential energy surface for the hydrogen shift in the vinyl irradical (C_2H_3) to vinylidyne (CH_3C) and from acetylene (C_2H_2) to vinylidene (H_2CC). We can see that the CH_3C isomer lies 198 kJ mol^{-1} above the vinyl radical, with the barrier to isomerism being 220 kJ mol^{-1} and, hence, 22 kJ mol^{-1} for the reverse process. Metropoulos (2003) calculated the same potential energy surface at the MRCI+Q level of theory;
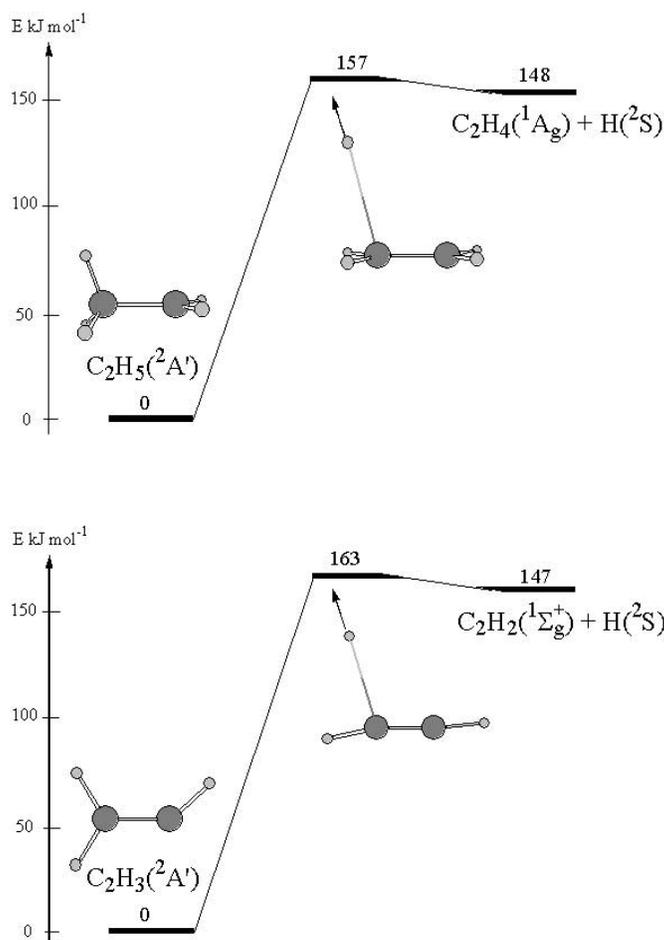
Fig. 9.—Same as Fig. 8, but for ethyl (C_2H_5; *top*) and vinyl (C_2H_3; *bottom*) calculated with the B3LYP/6-311G(d, p) level of theory. [*See the electronic edition of the Journal for a color version of this figure.*]

here, the CH_3C isomer was found to lie 204 kJ mol^{-1} above the vinyl radical isomer, with the barrier to isomerization being 236 kJ mol^{-1} (the reverse process has a barrier of 32 kJ mol^{-1}). In the bottom diagram, the acetylene molecule is 175 kJ mol^{-1} lower in energy than the H_2CC isomer, with the barrier to isomerism being 180 kJ mol^{-1}; this translates to only 5 kJ mol^{-1} for the reverse process. Kakkar et al. (2005) carried out calculations at the B3LYP/6-311++G(3df,3pd) level of theory; here, the H_2CC isomer was found to be 172 kJ mol^{-1} less stable, with a barrier of 182 kJ mol^{-1}, i.e., 10 kJ mol^{-1} for the reverse process. This is in contrast to an earlier study by Jursic (1999), who calculated that the H_2CC isomer lies 188 kJ mol^{-1} above the acetylene molecule; the calculated barrier was found to be less than 2 kJ mol^{-1}. Bittner & Köppel (2003) predict the barrier to be around 5 kJ mol^{-1}, based on a scanned CCSD(T)/cc-pVTZ potential surface. Finally, we investigated the potential energy surfaces of hydrogen atom elimination from the ethyl radical (C_2H_5; Fig. 9, *top*) and from the vinyl radical (C_2H_3; Fig. 9, *bottom*). Considering the ethyl radical, we see that the ethylene and hydrogen atom products are 148 kJ mol^{-1} above the ethyl radical; a small barrier of 9 kJ mol^{-1} exists for the reverse process. Mebel et al. (1995) found that the products lie around 140 kJ mol^{-1} higher in energy than the reactants, with a barrier for the reverse process of around 19 kJ mol^{-1}, compared to an experimental value of around 12 kJ mol^{-1}. Miller & Klippenstein (2004) found that the ethyl radical is 146 kJ mol^{-1} more stable than the products and the barrier to hydrogen elimination is around 158 kJ mol^{-1}, giving 12 kJ mol^{-1} for the reverse process, hydrogen addition to ethylene. In the bottom panel, where we investigate the hydrogen elimination from the vinyl radical, we find that the products, acetylene and a hydrogen atom, lie 147 kJ mol^{-1} above the vinyl radical, with a barrier of 163 kJ mol^{-1}, i.e., 16 kJ mol^{-1} for the reverse process of the hydrogen atom addition to the acetylene molecule. Miller & Klippenstein (2004) found that the vinyl radical is 145 kJ mol^{-1} more stable than the products with a barrier to hydrogen elimination of 163 kJ mol^{-1}, or 18 kJ mol^{-1} for the reverse process.

REFERENCES

Alman, D. A., Ruzic, D. N., & Brooks, J. N. 2000. Phys. Plasmas, 7, 1421
Baciocco, G., Calvani, P., & Cunsolo, S. 1987a, Int. J. IR Millimeter Waves, 8, 923
———. 1987b, J. Chem. Phys., 87, 1913
Baratta, G. A., Leto, G., & Palumbo, M. E. 2002, A&A, 384, 343
Becke, A. D. 1993, J. Chem. Phys., 98, 5648
Bennett, C. J., Jamieson, C. S., Mebel, A. M., & Kaiser, R. I. 2004, Phys. Chem. Chem. Phys., 6, 735
Bennett, C. J., Jamieson, C. S., Osamura, Y., & Kaiser, R. I. 2005, ApJ, 624, 1097

Bittner, M., & Köppel, H. 2003, Phys. Chem. Chem. Phys., 5, 4604
Boogert, A. C. A., et al. 2004, ApJS, 154, 359
Boudin, N., Schutte, W. A., & Greenberg, J. M. 1998, A&A, 331, 749
Brooke, T. Y., Tokunaga, A. T., Weaver, H. A., Crovisier, J., Bockelée-Morvan, D., & Crisp, D. 1996, Nature, 383, 606
Chapados, C., & Cabana, A. 1972, Canadian J. Chem., 50, 3521
Coustenis, A., Salama, A., Schulz, B., Ott, S., Lellouch, E., Encrenaz, Th., Gautier, D., & Feuchtgruber, H. 2003, Icarus, 161, 383
Cowieson, D. R., Barnes, A. J., & Orville-Thomas, W. J. 1981, J. Raman Spectrosc., 10, 224

Cravens, T. E., et al. 2005, Geophys. Res. Lett., 32, L12108
Cruikshank, D. P. 1998, Earth Moon Planets, 80, 3
d'Hendecourt, L. B., Allamandola, L. J., & Greenberg, J. M. 1985, A&A, 152, 130
Douté, S., Schmitt, B., Quirico, E., Owen, T. C., Cruikshank, D. P., de Bergh, C., Geballe, T. R., & Roush, T. L. 1999, Icarus, 142, 421
Drouin, D., Couture, A. R., Gauvin, R., Hovington, P., Horny, P., & Demers, H. 2001, Monte Carlo Simulation of Electron Trajectory in Solids (CASINO ver. 2.42; Sherbrooke: Univ. Sherbrooke)
Dunning, T. H. 1989, J. Chem. Phys., 90, 1007
Ehrenfreund, P., & Charnley, S. B. 2000, ARA&A, 38, 427
Ehrenfreund, P., Charnley, S. B., & Wooden, D. 2004, in Comets II, ed. M. C. Festou, H. U. Keller, & H. A. Weaver (Tucson: Univ. Arizona Press), 115
Frenklach, M., Wang, H., & Rabinowitz, M. J. 1992, Prog. Energy. Combustion Sci., 18, 47
Frisch, M. J., et al. 2001, Gaussian 98, rev. A.9 (Pittsburgh: Gaussian, Inc.)
Galabov, B., Yamaguchi, Y., Remington, R. B., & Schaefer, H. F., III. 2002, J. Phys. Chem. A, 106, 819
Gerakines, P. A., Bray, J. J., Davis, A., & Richey, C. R. 2005, ApJ, 620, 1140
Gerakines, P. A., Schutte, W. A., & Ehrenfreund, P. 1996, A&A, 312, 289
Gibb, E. L., Whittet, D. C. B., Boogert, A. C. A., & Tielens, A. G. G. M. 2004, ApJS, 151, 35
Grieger, S., Friedrich, H., Guckelsberger, K., Scherm, R., & Press, W. 1998, J. Chem. Phys., 109, 3161
Hasegawa, T. L, & Herbst, E. 1993, MNRAS, 263, 589
Hepp, M., & Herman, M. 1999, J. Mol. Spect., 197, 56
Irle, A., & Morokuma, K. 2000, J. Chem. Phys., 113, 6139
Jensen, J. H., Morokuma, K., & Gordon, M. S. 1994, J. Chem. Phys., 100, 1981
Johnson, R. E. 1990, Energetic Charged Particle Interactions with Atmospheres and Surfaces (Berlin: Springer)
Jones, A. P. 2005, in The Dusty and Molecular Universe, ed. A. Wilson (Noordwijk: ESA), 239
Jursic, B. S. 1999, J. Mol. Struc. (Theochem), 488, 87
Kaiser, R. I. 2002, Chem. Rev., 102, 1309
Kaiser, R. I., & Roessler, K. 1998, ApJ, 503, 959
Kakkar, R., Pathak, M., & Chadha, P. 2005, Int. J. Quantum Chem., 102, 189
Kerkeni, B., & Clary, D. C. 2005, J. Chem. Phys., 123, 064305
Khanna, R. K., & Ngoh, M. 1990, Spectrochim. Acta, 46A, 1057
Kim, G.-S., Nguyen, T. L., Mebel, A. M., Lin, S. H., & Nguyen, M. T. 2003, J. Phys. Chem. A, 107, 1788
Knyazev, V. D., Bencsura, A., Stoliarov, S. I., & Slagle, I. R. 1996, J. Phys. Chem., 100, 11346
Kobashi, K., Okada, K., & Yamamoto, T. 1977, J. Chem. Phys., 66, 5568
Lacy, J. H., Carr, J. S., Evans, N. J., II, Baas, F., Achtermann, J. M., & Arens, J. F. 1991, ApJ, 376, 556

Lee, C., Yang, W., & Parr, R. G. 1988, Phys. Rev. B., 37, 785
Marshall, M. D., & McKellar, A. R. W. 1986, J. Chem. Phys., 85, 3716
Mebel, A. M., Morokuma, K., & Lin, M. C. 1995, J. Chem. Phys., 103, 3440
Metropoulos, A. 2003, Chem. Phys. Lett., 368, 701
Miller, J. A., & Klippenstein, S. J. 2004, Phys. Chem. Chem. Phys., 6, 1192
Moore, M. H., & Hudson, R. L. 1998, Icarus, 135, 518
———. 2003, Icarus, 161, 486
Moore, M. H., Hudson, R. L., & Gerakines, P. A. 2001, Spectrochim. Acta A, 57, 843
Mumma, M. J., DiSanti, M. A., Dello Russo, N., Fomenkova, M., Magee-Sauer, K., Kaminski, C. D., & Xie, D. X. 1996, Science, 272, 1310
Mumma, M. J., DiSanti, M. A., Dello Russo, N., Magee-Sauer, K., Gibb, E., & Novak, R. 2003, Adv. Space Res., 31, 2563
Nakamoto, K. 1997, Infrared and Raman Spectra of Inorganic and Coordination Compounds A (5th ed.; New York: Wiley)
Nakano, T., Toyoda, H., & Sugai, H. 1991, Japanese J. Appl. Phys., 30, 2908
Okabe, H. 1978, Photochemistry of Small Molecules, (New York: Wiley)
Pacansky, J., & Bargon, J. 1975, J. Amer. Chem. Soc., 97, 6896
Pearl, J., Ngoh, M., Ospona, M., & Khanna, R. 1991, J. Geophys. Res. (Planets), 96, 17477
Prasad, S. S., & Tarafdar, S. P. 1983, ApJ, 267, 603
Purvis, G. D., & Bartlett, R. J. 1982, J. Chem. Phys., 76, 1910
Raghavachari, K., Trucks, G. W., Pople, J. A., & Head-Gordon, M. 1989, Chem. Phys. Lett., 157, 479
Roush, T. L. 2001, J. Geophys. Res., 106, 33315
Ruffle, D. P., & Herbst, E. 2001, MNRAS, 322, 770
Sasaki, T., Kanno, A., Ishiguro, M., Kinoshita, D., & Nakamura, R. 2005, ApJ, 618, L57
Sherrill, C. D., Byrd, E. F. C., & Head-Gordon, M. 2000, J. Chem. Phys., 113, 1447
Snelson, A. 1970, J. Phys. Chem., 74, 537
Strazzulla, G., & Johnson, R. E. 1991, in Comets in the Post-Halley Era, ed. R. L. Newburn, Jr., M. Neugebauer, & J. Rahe (Dordrecht: Kluwer), 243
Tran, B. N., Joseph, J. C., Force, M., Briggs, R. G., Vuitton, V., & Ferris, J. P. 2005, Icarus, 177, 106
Vernazza, P., Mothé-Diniz, T., Barucci, M. A., Birlan, M., Carvano, J. M., Strazzulla, G., Fulchignoni, M., & Migliorini, A. 2005, A&A, 436, 1113
Weaver, H. A., Brooke, T. Y., Chin, G., Kim, S. J., Bockelée-Morvan, D., & Davies, J. K. 1999, Earth Moon Planets, 78, 71
Wormhoudt, J., & McCurdy, K. E. 1989, Chem. Phys. Lett., 156, 47
Wu, T., Werner, H-J., & Manthe, U. 2004, Science, 306, 2227
Wyckoff, R. 1965, Crystal Structures 4 (New York: Wiley)
Zeigler, J. F., Biersack, J. P., & Littmark, U. 1985, The Stopping and Range of Ions in Solids (New York: Permagon)
Zhang, Y., Li, Q. S., & Zhang, S. 2004, J. Molec, Struc. (Theochem), 682, 163
Zhitnikov, R. A., & Dmitriev, Y. A. 2002, A&A, 386, 1129